 doi:10.20944/preprints202107.0647.v1

Article

Graphene – diamond nanomaterials: a status quo review

Jana Vejpravová [1,*]

1 Department of Condensed Matter Physics, Faculty of Mathematics and Physics, Charles University, Ke Karlovu 5, 121 16 Prague 2, Czech Republic.

* Correspondence: JV, jana@mag.mff.cuni.cz

Abstract: Carbon nanomaterials with a different character of the chemical bond – graphene (sp^2) and nanodiamond (sp^3) are the building bricks for a new class of all-carbon hybrid nanomaterials, where the two different carbon networks with the sp^3 and sp^2 hybridization coexist, interact and even transform into one another. The unique electronic, mechanical, and chemical properties of the two border nanoallotropes of carbon ensure the immense application potential and versatility of these all-carbon graphene – diamond nanomaterials. The review gives an overview of the current state of the art of graphene – diamond nanomaterials, including their composites, heterojunctions, and other hybrids for sensing, electronic, energy storage, and other applications. Also, the graphene-to-diamond and diamond-to-graphene transformations at the nanoscale, essential for innovative fabrication, and stability and chemical reactivity assessment are discussed based on extensive theoretical, computational, and experimental studies.

Keywords: graphene; diamond; nanodiamond; diamane; graphene-diamond nanomaterials; all carbon materials; electrochemistry; mechanochemistry; sensor; supercapacitor; field-effect transistor; detector; superlubrication; tribology; graphene-diamond phase transformation

1. Introduction

Carbon is one of the essential elements on our planet; not only do all living species contain carbon but also its pure forms exhibit unique properties. The arrangement of the carbon atoms are adopted in space can be very different, thus making a number of the possible structural variants the carbon allotropes (shown in Figure 1(a)) with differing properties arising from their special chemical bonding and crystal structures. The hybridization of the carbon atom determines the most prominent types of arrangement – either sp^2 giving rise to a strictly planar configuration or sp^3 suggesting tetrahedral coordination. The two border structures represent the most known allotropes: graphite and diamond.

In a diamond, each carbon atom is attached to four other carbon atoms 1.544 Å away with a C-C-C bond angle of 109.5°. It is a strong, rigid three-dimensional structure that results in an infinite network of atoms. This accounts for the diamond's hardness, extraordinary strength, and durability and gives the diamond a higher density (3.514 g/cm^3) than graphite (2.266 g^{-1}cm^3). Because of its tetrahedral coordination, diamond also shows excellent resistance to compression. Diamond is the most rigid material known (designated as ten on the Mohs scale). It is one of the best conductors of heat, with heat conductivity up to five times higher than copper. Diamond also conducts sound, but not electricity; it is an insulator, and its electrical resistance, optical transmissivity, and chemical inertness are correspondingly remarkable.

The carbon atoms in graphite are also arranged in an infinite array, but they are layered. Each carbon atom is bonded to three other carbon atoms and positioned at the corners of a network of regular hexagons with a 120° C-C-C bond angle. These planar arrangements extend in two dimensions to form a horizontal, hexagonal array held together by weaker forces known as stacking interactions. The distance between the two layers is longer (3.347 Å) than the distance between carbon atoms within each planar layer (1.418

 doi:10.20944/preprints202107.0647.v1

Å). Unlike diamond, graphite can be used as a lubricant because the layers cleave readily. It is soft and slippery, and its hardness is less than one on the Mohs scale. The planar structure of graphite allows electrons to move easily within the planes, thus permitting the graphite to conduct electricity and heat and absorb light.

In addition to the most prominent allotropes incorporating the two border hybridization possibilities, the carbon atoms form additional configurations in space, especially when approaching nanoscale (see Figure 1(a). The most explored nanocarbon species are the graphene (GN) and the nanodiamond (ND), directly derived from the structures of the macroscopic parent phases. The latter two types of nanocarbons are in the spotlight of current science thanks to their colossal application potential given by the unique fundamental physics behind them corroborated with multifaceted modification possibilities utilizing green chemistry.

Graphene is still believed to be a miracle material due to its straightforwardness [1]. It is the thinnest compound known to man kind (with a single atom thickness), the lightest material, the strongest compound discovered, the best conductor of heat at room temperature, and the best electricity conductor. Other notable properties of graphene are its unique levels of light absorption at about 2.3 % of white light. As graphene has been predicted to be much more efficient at conducting electrons than silicon and can transfer electrons much faster, another utilization of this material is flexible, robust touchscreen devices such as mobile smartphones and wrist watches.

Recently, graphene entered the energy storage scene as an excellent candidate for the construction of batteries and supercapacitors [2]. In initial tests carried out, laser-scribed graphene supercapacitors were shown to offer power density comparable to high-power lithium-ion batteries in use today. Regarding other opportunities, sp^2 nanocarbon-based materials have been employed in various types of sensors [3] and nanoelectronics devices [4,5]. However, the quality of graphene still prevails to be the limiting factor in technological applications.

Obviously, the properties of graphene, however unique, are substantially influenced by their immediate environment—molecules in the surrounding atmosphere as well as atoms in the substrate transfer charge to the material. The extreme susceptibility to the ambiance can be a bottleneck and an excellent opportunity to boost these unique materials' applicability further.

Despite a tiny energy difference between the equilibrium structural arrangement of the graphite and the diamond, the latter is not favored at ambient conditions, regardless of downscaling the particle size to nanometer dimensions [6]. However, the outstanding physio-chemical properties of the diamond make this carbon allotrope also a highly demanding material for various applications.

The NDs are unique among nanomaterials due to their combination of outstanding mechanical performance, chemical resistance, biocompatibility, and exceptional optical and electronic properties [7,8].

NDs also provide unique spectral features unattainable in the molecular world, such as color centers embedded in nanoparticle crystal lattices, suggesting their use in diagnostic and imaging approaches in biomedicine as sophisticated optical tools. These nitrogen-vacancy (NV) centers can respond to changes in the nanoparticle environment with exceptional sensitivity and report on various local variables. Thus the NV centers can be used to construct attractive nanosensors because NV center offers a unique sensitivity to the extremely weak electric and magnetic field at a nanoscale resolution [9–11].

Similarly, as in case of the graphene, the performance of NDs is strongly influenced by structural features such as the particle size, shape, crystallographic order, chemical functionalization of the surface layer, level of internal defects and dopants, and presence of sp^2 carbons in the particle shell [8].

In this vein, mitigation of the effects of physio-chemical limits and sample quality by creating novel all-carbon nanomaterials appeared to be a very promising direction. Owing to the exceptional properties of sp^2 graphene (like Young' modulus, strength, thermal and

 doi:10.20944/preprints202107.0647.v1

electrical conductivity, etc.) and sp^3 diamond (chemical stability, hardness, thermal conductivity), it is also appealing to combine those nanocarbon allotropes in a new generation of nanoelectronics and optoelectronic devices, various functional composites, heterostructures, and networks. The most promising directions are summarized in the scheme presented in Figure 1(b).

This review aims to summarize important aspects of the current graphene – diamond nanomaterials' research. The structure of the review is as follows. First, phase transformation between the graphene and diamond at the nanoscale is discussed in section 2. This section also concerns mutual phase transformations and the use of diamond as a substrate for graphene growth and vice versa. Second, graphene–diamond heterostructures developed for sensing applications are described in section 3. Third, the graphene-diamond heterojunctions are discussed from the point of view of tribology and nanoelectronics in section 4. Graphene – diamond-based nanomaterials developed for other exciting applications such as energy storage, materials' processing, detectors, and light sources, catalysts, and nanoscale pressure devices are summarized in section 5. Finally, a summary and future prospects of the graphene–diamond nanomaterials are given in section 6.

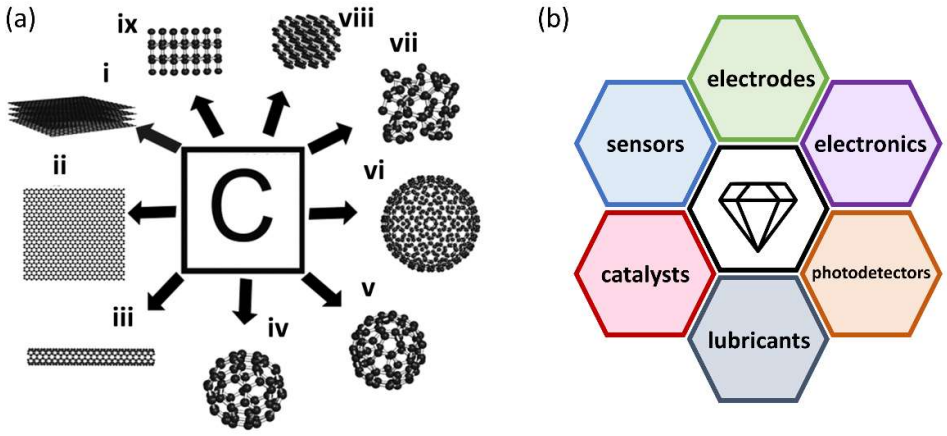

Figure 1. (a) Different carbon allotropes: (i) graphite, (ii) graphene, (iii) carbon nanotube, (iv) fullerene C_{60}, (v) C_{70}, (vi) C_{540}, (vii) amorphous carbon, (viii) lonsdaleite, and (ix) diamond. (b) Schematic presentation of the application areas of the graphene – diamond nanomaterials.

2. Graphene – diamond phase transformations at nanoscale

Although the energy difference between the parent bulk carbon allotropes, graphite and diamond is only 0.02 eV / atom, an activation barrier required for the phase transformation is 0.4 eV, and the conversion of graphite to diamond occurs under extreme pressures and temperatures. However, for ND particles (3-6 nm), tetrahedral coordination is preferred, which makes the stabilization of NDs easier [6]. Thus, the sp^2 – sp^3 transformations at the nanoscale are the most important processes governing the final materials' stability, reactivity, and physical properties. Selection of first principle studies and modeling, and experimental conditions, and difficulties of the peculiar sp^2 – sp^3 all-carbon phase transitions will be discussed in this section.

3.1. First principle calculations and modelling

First, the transformation of graphene and derived systems to diamond-like structures will be discussed.

Alekseev investigated the transformation of the upper sublayer of carbon atoms in the lattice of single-crystal diamond into a flat graphene lattice under the influence of the atoms of a molten copper film on the diamond surface by a quantum-chemical simulation

 doi:10.20944/preprints202107.0647.v1

[12]. He reported that the stable configuration corresponds to the thermally activated motion of carbon atoms in the lower sublayer of the interface diamond layer to the position of graphene, i.e., at the same level as the atoms of the upper sublayer.

Kvashnin et al. explored how few-layer graphene can undergo phase transformation into a thin diamond film under reduced pressure if the process is facilitated by hydrogenation of the surfaces [13]. The authors concluded that such a "chemically-induced phase transition" is an inherently nanoscale phenomenon when the surface conditions directly affect thermodynamics, and the transition pressure depends greatly on film thickness. They also suggested a pressure-temperature phase diagram of quasi-2D diamond - multilayered graphene system, which accurately describes the role of film thickness and shows the feasibility of creating novel quasi-2D materials.

Paul and Momeni studied the mechanochemistry of the phase transformation of the diamond thin films as a function of the layer thickness at different pressures and temperatures for pristine and hydrogenated multilayer graphene [14] theoretically. In agreement with other studies, the results indicate that the transformation conditions depend on the number of graphene layers and surface chemistry. Although the pristine multilayer graphene to diamond transformation is reversible, hydrogenated multilayer graphene structures had formed a metastable diamond film.

Antipina and co-workers reported that depending on the functionalization of few-layer graphene with H (H_2), F (F_2), NH_3, and H_2O, spontaneous conversion to either cubic or hexagonal diamond films with a specific surface and well-defined properties can be achieved [14].

Belenkov et al. suggested forming a geometrically optimized structure of ten carbon diamond-like phases obtained by crosslinking the graphene layers [15]. They also calculated X-ray powder diffraction patterns, which can be used to identify these new phases.

Reactive molecular dynamics simulations revealed that bilayer graphene transforms into a diamond-like film, while the three- to six-layer graphene with AB layer stacking fail to form a diamond-like film up to 200 GPa. The study also suggests that the ABA layer stacking is directly related to the hindering of the chain structure formation and the suppression of the transformation. Surprisingly, the bond-chain-structure transformation mechanism is effective in three-layer graphene with ABC layer stacking and five-layer graphene with ABCAB layer stacking. Thus, the stacking faults are effective catalysts for the high-pressure transformation of multilayer graphene to diamond [16].

Also, it has been demonstrated that the diamond can be transformed into graphene.

For example, spontaneous graphene-like stripes on the reconstructed surface are expected to occur on high-index diamond C(331) surface [17]. Van Wijk and Fasolino demonstrated via molecular dynamics simulations that the transformation from diamond to amorphous carbon from sliding under pressure could be prevented by having at least two graphene layers between the diamond slabs [18].

The graphene to diamond transformation may also yield exotic novel phases, see Table 1 and Figure 2. For example, Cellini et al. found that under localized pressure, two-layer epitaxial graphene behaves as an ultra-hard and ultra-stiff coating, showing exceptional mechanical properties that far exceed those of bare SiC. DFT calculations indicate that this unique behavior stems from an sp^2 to sp^3 reversible phase transition of carbon films under compression, leading to a single-layer diamond-like structure, the diamane [19], Figure 2(a).

Erohin et al. carried out thermodynamic theory coupled with atomistic first-principles computations to predict the nucleation barriers, definitive for the kinetic feasibility of diamane formation [20]. They also reported that the optimal adsorbent chair pattern on bilayer graphene results in a cubic diamond lattice. In contrast, for thicker precursors, the adsorbent boat structure produces hexagonal diamonds (lonsdaleite). H and F support graphene to the diamond formation, while Cl appears sterically hindered.

 doi:10.20944/preprints202107.0647.v1

Table 1. Exotic nanocarbon phases and architectures due to graphene-diamond reconstruction at the nanoscale.

System	Evidence	References
Diamane	Atomistic first principles computations	[21]
F-diamane	XPS/UPS, Raman spectroscopy	[22]
H-diamane	Optical absorption, XRD	[23]
LA10 phase	DFT	[24]
Graphene Arch-Bridge	First principle calculations	[25]
Diaphite	DFT, HR TEM	[26–28]

The graphene growth directly out of diamond (111) by B doping was studied by Gu et al. [29]. The spontaneous graphene formation occurred due to the reconstruction of the diamond surface when the B doping density and profile are adequate. A similar problem was addressed by Lu et al. [30]. Boron-doping-induced surface reconstruction was also identified as the critical mechanism responsible for the diamond-to-graphene phase transition.

Okada investigated the formation of graphene nanostructures on diamond nanowires with nanometer-scale diameters up to 4.3 nm by first-principle total-energy calculations [31]. He suggested that a surface reconstruction results in graphitization of the outermost shell of the wire, which is expected to cause the structural transformation from diamond to the multi-shell nanotube or nano-scale graphene ribbons. The electronic structures of the wires are semiconducting with a moderate indirect energy gap.

A very interesting computational study by Greshnyakov et al. suggests the formation of a carbon diamond-like LA10 phase, in which all the atomic positions are crystallographically equivalent [24]. The most probable synthetic way to obtain the LA10 phase is a strong static compression of graphite, consisting of tetragonal polymorphic variety graphene, perpendicular to the graphene layers. The diamond-like LA10 phase structure can be theoretically derived by polymerization of tetragonal L4-8 graphene layers, consisting of four-membered and eight-membered structural units. The LA10 crystalline phase lattice belongs to a tetragonal crystal system with $I4_1/amd$ space group symmetry. The body-centered tetragonal unit cell has the following parameters: a = 3.581 Å, c = 8.611 Å, and Z = 16 atoms. Band structure and electron density of states calculations showed that the diamond-like LA10 phase is a wide-gap semiconductor with a band gap of 5.0 eV to 6.1 eV.

Despite their widespread use in high-pressure experiments, little is known about carbon-containing materials' physical and chemical properties as they expand and cool to ambient conditions. Ileri et al. suggested that nanodiamonds can be stabilized when carbon-containing materials expand and cool to ambient conditions [32]. Their quantum simulations investigated such processes during shock compression. Expansions from three different sets of shock conditions yielded various chain and ring structures, and the relative amounts of graphite-like and diamond-like particles formed during cooling and equilibration were evaluated. Although the graphene sheets are the majority product, increasingly larger amounts of diamond particles are formed [32].

Preprints (www.preprints.org) | NOT PEER-REVIEWED | Posted: 29 July 2021 doi:10.20944/preprints202107.0647.v1

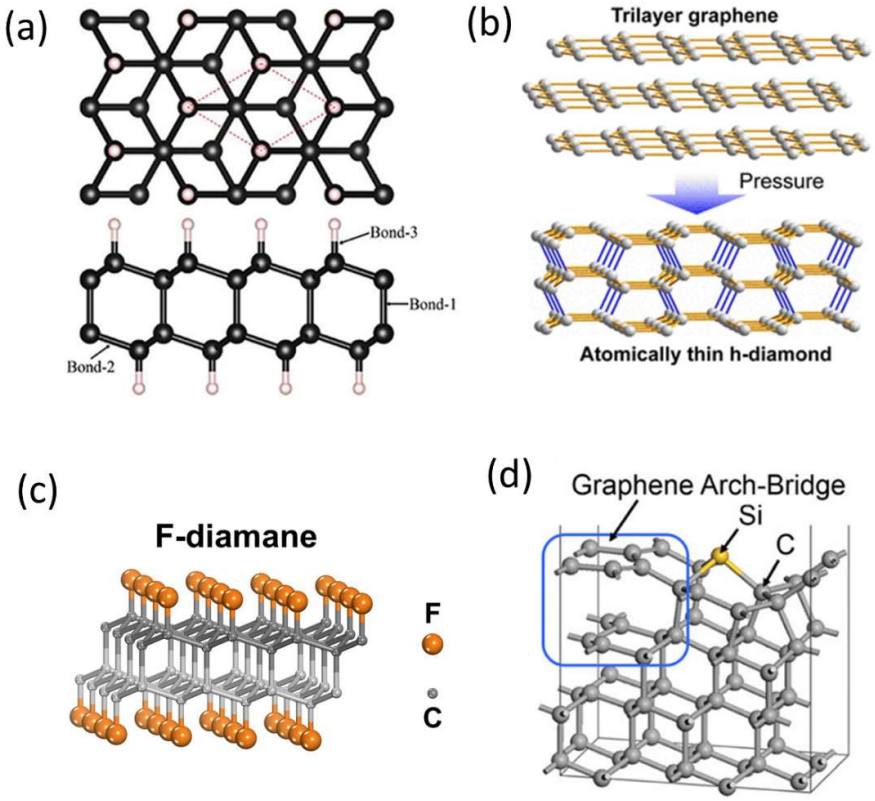

Figure 2. Examples of graphene – diamond transformations at nanoscale. (a) fully optimized structure of diamane. Reprinted (adapted) with permission from Hu, Y.X.; Li, D.F.; Yin, Y.; Li, S.C.; Ding, G.Q.; Zhou, H.B.; Zhang, G. The important role of strain on phonon hydrodynamics 1076 in diamond-like bi-layer graphene. *Nanotechnology* **2020**, *31*, doi:10.1088/1361-6528/ab8ee1. Copyright 2020 IOP publishing. (b) pressure-induced graphene to H-diamane transformation. Reprinted (adapted) with permission from Ke, F.; Zhang, L.; Chen, Y.; Yin, K.; Wang, C.; Tzeng, Y.K.; Lin, Y.; Dong, H.; Liu, Z.; Tse, J.S.; et al. Synthesis of Atomically Thin Hexagonal Diamond with Compression. *Nano Lett.* **2020**, *20*, 5916–5921. Copyright 2020 American Chemical Society. (c) F-diamane (adapted from https://www.techexplorist.com/converting-graphene-diamond-film/28444/), and (d) Graphene Arch-Bridge. Reprinted (adapted) with permission from Bai, S.D.; Xu, J.X.; Wang, Y.; Zhang, Q.; Tsuruda, T.; Higuchi, Y.; Ozawa, N.; Adachi, K.; Martin, J.M.; Kubo, M. Generation 1059 of "Graphene Arch-Bridge" on a Diamond Surface by Si Doping: A First-Principles Computational Study. *J. Phys. Chem. C* 1060 **2020**, *124*, 26379–26386. Copyright 2020 American Chemical Society.

The relationship between the deposition condition and quality of diamond-like carbon on top of multilayer graphene was also investigated by molecular dynamics simulations [33]. An increase in the number of dangling bonds at the interface between the top graphene layer and the diamond-like film indicates that a decrease of the incident energy reduces the adhesion quality of the diamond thin film on graphene. Analysis of radial distribution function indicates that sp^3 hybridized carbon atoms tend to grow near already existing sp^3 atoms. This explains why the quality of the diamond-like structures grown on graphene generally has a lower content of sp^3 C atoms than those produced directly on the diamond. Ring analysis further shows that a DLC structure grown on the sp^2-rich structures like graphene contains a higher fraction of disordered ring structures.

Recently, two new families of diamond-graphene (diaphite) phases constructed from layered and bonded were reported [26]. These nanocomposite structures are identified within both natural impact diamonds and laboratory-shocked samples and possess diffraction features that have previously been assigned to lonsdaleite and post-graphite phases. The diaphite nanocomposites represent a new class of high-performance carbon

 doi:10.20944/preprints202107.0647.v1

materials that are predicted to combine the superhard qualities of diamond with high fracture toughness and ductility enabled by the graphitic units and the atomically defined interfaces between the sp^3- and sp^2-bonded nanodomains.

Finally, new nanosized architectures linking the structure of graphene and diamond were also reported. Bai and co-workers suggested a formation of the so-called "Graphene Arch-Bridge" (Figure 2(d)), which can be stabilized on a diamond (111) surface by Si doping. Their first principle calculations revealed that the significant stress around the doped Si atom leads to the transition of the six-membered C ring to a five-membered C ring associated with the sp^3 to sp^2 change. The authors also proposed that the "Graphene Arch-Bridge" is responsible for the experimentally observed super-low friction of Si-doped diamond-like carbon.

3.2. Experimental demonstration and growth mechanism

As discussed in the previous subsection, many first-principle and computational studies on the transformation of graphene into a diamond-like film were carried out to date. However, in general, these studies suggest that atomically thin diamond films are not achievable in a pristine state because diamonds possess a three-dimensional crystalline structure and would lack chemical stability when thinned down to the thickness of the diamond's unit cell due to the dangling sp^3 bonds. Thus, chemical functionalization of the surface carbons with specific chemical groups was considered necessary to stabilize the two-dimensional structure, such as surface hydrogenation or fluorination, and various substrates have also been used in these synthesizing attempts. A first convincing experimental proof of such a conversion was delivered by Bakharev and co-workers [22]. They observed that fluorination of Bernal (AB)-stacked bilayer graphene grown by chemical vapor deposition on a single-crystal CuNi(111) surface results in a fluorinated diamond monolayer ('F-diamane'), see Figure 2(c). A similar structure, the so-called H-diamane, was obtained by pressure-induced transformation of few-layer graphene [23], see Figure 2(b).

Carvalho reported on simultaneous growth of graphene and nanocrystalline diamond by the microwave plasma chemical vapor deposition technique on copper. Additionally, HR TEM analysis permitted to detail the diamond nanocrystalline structure, revealing a close link to the graphene layer on the basis of which a diamond on graphene nucleation mechanism was proposed [34]. The formation of high-quality graphene layers on the diamond was also achieved based on a high-temperature annealing method using a Cu catalyst [35].

Ordered graphene films have been fabricated on Fe-treated SiC and diamond surfaces using the catalytic conversion of sp^3 to sp^2 carbon. This new approach enabled epitaxial graphene to be grown on a diamond surface for the first time. Also, graphene is only formed on treated regions of the surface, convenient for patterning graphene structures on SiC and diamond at industrially realistic temperatures [36,37]. Also, multilayer graphene can be grown by precipitation upon cooling of a thin nickel film deposited by e-beam evaporation on single crystal diamond (001) oriented substrates. The nickel acts as a strong catalyst inducing the dissolution of carbon from diamond into the metal. Carbon segregation produces multilayers of graphene on the top surface. This method provides a venue for the fabrication of large-area graphene films [38]. Multilayer graphene films with some monolayer coverage were also grown on atomically flat diamond (111) surfaces via annealing with nickel as a catalyst [39].

Berman and co-workers introduced a direct approach to transforming polycrystalline diamond into high-quality graphene layers on a wafer scale using a rapid thermal annealing process facilitated by a nickel thin film catalyst on top [40]. In addition, they demonstrated the lateral growth of free-standing graphene over micron-sized pre-fabricated holes, which is a critical technological step for large-scale graphene/diamond-based electronics production. Surface transformations of carbon deposited on polycrystalline nickel by hot filaments chemical vapor deposition were experimentally investigated by Rey and

 doi:10.20944/preprints202107.0647.v1

Normand [41]. First, graphene and a highly graphitic layer form, then multiphase formation with graphitic/carbidic and diamond-like carbon occur. Finally, at a critical temperature that strongly depends on the pretreatment of the polycrystalline nickel surface, a rapid transition to the diamond island takes place. Whatever the substrate, the diamond is always the final product, and some graphene layers are the initial product.

Taking advantage of the Ni-assisted diamond transformation, Tsubota et al. proposed a new simple method for fabricating a microchannel covered with a graphene layer on a diamond substrate [42]. Also, Ni/Fe catalyst-assisted process enables growth of graphene nanowalls directly on diamond particles by a simple heat-treatment process in a vacuum induction furnace [43].

The iron powder was used as a catalyst for the growth of single-crystalline 3C-SiC nanowires directly on the surface of the bulk diamond by heating treatment at 1300 °C. The graphene served as the second carbon source during the reaction. A graphene-assisted growth model to interpret the growth process of SiC nanowires on the diamond surface was also proposed [44].

A novel approach is proposed by Li et al., which grows diamond on graphene quasi-homogeneous epitaxial substrate [45]. The high-quality diamond was synthesized on a quasi homoepitaxial graphene substrate through sp^2-sp^3 hybridization and covalent bond transformation. An internal space microstructure network of carbon atoms was produced through different non-covalent interactions. At last, graphene is converted into the diamond. This process can also be used to synthesize hydrophilic porous diamond film. It is a promising approach to the development of new graphene/diamond-based components in the future.

Hussain et al. suggested that applying the Hummer method on graphene oxide with an ultrasound exposure time of 20 min and 2 h can result in graphene oxide formation and nanodiamond formation, respectively [46]. The diamond-like carbon can also be transformed into graphene and reduced graphene oxide by nanosecond pulsed laser annealing [47].

Hembram et al. achieved a carbon-pure formation of the diamond via surface hybridization with graphene [48]. Graphene layers (5-50 nm in thickness) were grown vertically onto a polished < 110 > textured polycrystalline diamond plate at similar to 1300 °C via hydrogen plasma etching in a chemical vapor deposition chamber. Due to the crystallographic relationship, the graphene layers embed at an angle of 30° to the diamond surface comprising the (110) planes.

Interestingly, diamond aerogel was obtained by laser heating graphene aerogel under high pressure in a diamond anvil cell [49]. It was also possible to tune the microstructures of diamond aerogel by controlling the synthesis of graphene precursors.

The regularities of forming hetero-graphene and hetero-diamond phases were studied in the pressure range of 4-12 GPa at thermobaric treatment of mixtures of carbon nitride or melamine boron by Filonenko et al. [50]. The authors concluded that phase transition to a diamond-like phase does not require the use of catalysts. Fukuda and co-workers also suggested that a high temperature and high pressure-driven crystallization of two-dimensional graphene oxide (GO) nanosheets reveals three-dimensional diamond [51].

To clarify the graphene formation process on a diamond C(111) surface, changes in the chemical bonding state caused by annealing in a vacuum were investigated by photoelectron spectroscopy using synchrotron radiation [52]. The authors found that graphitization on the diamond C(111) surface began at approximately 1120 K, lower than that for a SiC substrate. The obtained photoelectron spectra indicated that a buffer layer composed of sp^2-bonded carbon atoms existed at the interface between graphene and the diamond C(111) surface. The formation of a graphene-on-diamond structure by the graphitization of a diamond (111) surface was also reported by Tokuda and co-workers [53]. Before the graphitization, atomically flat diamond (111) surfaces were formed by homoepitaxial lateral growth.

 doi:10.20944/preprints202107.0647.v1

The transition between the semiconducting and metallic properties of graphene - diamond-like carbon heterostructures was investigated by Zhao and co-workers [54]. The results show that different graphene terminations (N, F) strongly affect the electronic properties of the graphene heterostructures. GN-F-DLC samples displayed p-type of doping and considerably higher mobility, while the GN-N-DLC samples supported higher carrier densities, being almost metallic.

The graphene-induced growth of diamond films can also be achieved on tungsten [55]. Heterogenous diamond nucleation, assisted by sp^3 C-W bonds, takes place along the edge line of graphene on tungsten leading to the deposition of continuous diamond films.

As an unusual alternative, low-energy Ar ion beam modification was proposed to create graphene on the top of the insulating diamond-like carbon films [56,57]. In such a low-temperature process, the surface of the amorphous carbon could crystallize to graphene as a result of point defect creation and enhanced diffusion caused by the ion bombardment.

3. Graphene – diamond sensors and biosensors

Graphene and graphene-oxide (GO) based electrodes combined with NDs and more complex nanomaterials based on the all-carbon networks were identified as great and versatile platforms for the construction of various types of sensors. Among them, the most recognized are the electrochemical sensors and biosensors. An overview is given in Table 2, and selected cases are discussed hereafter.

Table 2. Overview of graphene-diamond-based nanomaterials for various sensing applications.

System	Application	References
RGO/BDND	Protein sensor	[58]
Diamond/G nanoplatelets/Pt nanoparticles	L-Glutamate electrochemical sensor	[59]
Ni nanoparticle-modified G-diamond hybrid	Glucose sensor	[60]
Plasmonic gold nanostructure/diamond-like film	SERS sensor	[61]
Vertical G sheets/separated papillary granules on ND films	ORR electrode	[62]
BD diamond/G nanowalls electrode	Detection of explosives	[63]
G/diamond electrode	Enantiomer recognition	[64]
GN/BDND electrodes	Epinephrine detection	[65]
GO/BD-diamond electrode	Tetracycline detection	[66]
GN/BD-diamond electrodes	Electrochemical sensing of trace Pb^{2+} in seawater	[67]
diamond, GN, and polyaniline/GC electrode	Electrochemical sensing of 2,4-dichlorophenol	[68]
N-UNCD/MLGN film	Electrochemical sensor (Ag^{+})	[69]
(Ag)GN-modified BD-diamond electrode	Electrochemical sensor of pesticides	[70,71]
GN/BD-diamond electrodes	Electrochemical sensor of biomarkers	[72]
Few-layer GN/HPHT diamond electrode	Dopamine detection	[73]

 doi:10.20944/preprints202107.0647.v1

3.1. Electrochemical sensors

Electrochemical sensors based on graphene-diamond hybrid nanomaterials are highly competitive for various applications.

Electrochemical determination of nitroaromatic explosives at boron-doped diamond/graphene nanowall electrodes was proposed by Dettlaff and co-workers [63,74]. The limit of detection was as low as 0.52 ppm thanks to the electrochemical performance of the diamond/graphene composite nanowall surface.

Gao et al. proposed a highly stable and regenerative graphene/diamond electrode as an enantiomer recognition platform after a simple beta-cyclodextrin drop-casting process [64]. The proposed enantiomer recognition sensor has been successfully used for D and L-phenylalanine recognition. In addition, the electrode can be simply regenerated by half-minute sonication due to the strong interfacial bonding between graphene and diamond. Therefore, the proposed electrode showed significant potential as a reusable sensing platform for enantiomer recognition.

Also, a series of nanocrystalline diamond and graphene hybridized films with various morphologies and compositions of grain boundaries was investigated for application as an electrode material [75]. The films were grown by adjusting the growth pressure by hot-filament chemical vapor deposition. It is concluded that the high diamond content is beneficial to enlarge the potential windows and decrease the background current, and the graphene components take advantage of improving the redox current. Moreover, the ordered and small graphene surrounding the diamond grains is positive to improve the electrochemical response without the rising background current.

The same authors reported constructing a more efficient air/solid/solution tri-interface for carbon-based oxygen reduced reaction (ORR) electrodes [62]. They have successfully assembled vertical graphene sheets with edge defects as catalyst centers on separated papillary granules formed nanocrystalline diamond films. They also prepared high hydrophobic and high sticky carbon-based electrodes with highly efficient ORR performance. They demonstrated that hydrophobic to the super-hydrophobic surface can be tuned by the tilt of the vertical graphene flakes. The study suggests a simple way to construct catalytically active vertical graphene sheets on nanocrystalline diamond films.

Hybrid systems based on graphene and diamond containing another functional nanomaterial have also been recognized. For example, close-packed 2D assembly of plasmonic gold nanostructure was fabricated on a diamond-like carbon film by two-step electrodeposition via reduced graphene oxide modulation [61]. The oxygen functionalities at the RGO surface which were controlled by changing the electrochemical reduction time of GO, provided reactive sites for nucleation and growth of gold nanoparticles. The Raman intensity of rhodamine B obtained from the gold assembly showed an 860-fold increase compared with that from Si reference, indicating a coupling of localized electromagnetic field enhancement and chemical enhancement. The platforms have potential applications in biochemical analysis, environmental monitoring, disease detection, and food safety.

A new electrochemical sensor designed by modifying the commercial boron-doped diamond electrode with graphene oxide reduced electrochemically and further electrode coated with silver (Ag/GO/BDD) electrode was selected to detect tetracycline in aqueous solution.

Pei and co-workers improved the repeatability and lifetime of a sensor for the electrochemical detection of trace Pb^{2+} in seawater using graphene-functionalized self-supported boron-doped diamond (G/SBDD) electrode [67].

A novel ternary composite electrode made from diamond, graphene, and polyaniline was designed for the electrochemical determination of 2,4dichlorophenol in aqueous media [68]. The composite was obtained through oxidative polymerization of aniline in the presence of graphene and diamond. For the application, a glassy carbon electrode (GC) was modified with this nanocomposite. The obtained results show that the modified electrode exhibits superior electrochemical properties to the bare GC electrode.

 doi:10.20944/preprints202107.0647.v1

Electrochemical detection of Ag^+ using a novel nitrogen-incorporated ultrananocrystalline diamond/multilayer graphene (N-UNCD/MLGN) composite carbon films was reported by Peng et al. [69]. The films were deposited on silicon substrates via a microwave plasma chemical vapor deposition method, in which diethylamine was utilized as the sole carbon and nitrogen source. In the composite films, MLGNs are grown vertically on the substrate surface and interlaced together to build a porous nest-like morphology. These N-UNCD/MLGN films process large electrochemical double-layer capacitance (EDLC) and robust cyclic stability, which make them a new class of carbon-based electrodes for the application in electrochemical energy storage and/or electrochemical sensing.

Novel graphene-modified boron-doped diamond electrode and silver/graphene-modified boron-doped diamond electrode were obtained to determine carbaryl and paraquat pesticides selectively from aqueous solution [70,71]. Compared with the graphene-modified boron-doped diamond electrode [71], the Ag-boosted electrode exhibited excellent electrocatalytic activity towards carbaryl electrooxidation and paraquat electroreduction [70]. Also, a proof-of-concept was demonstrated by the application in the real surface water sample.

To complete the puzzle of the outstanding electrochemical properties of the diamond-graphene nanomaterials, synergistic antibacterial activity of reduced graphene oxide and boron-doped diamond anode in a three-dimensional electrochemical oxidation system was reported [76].

3.2. Biosensors

Hybrid graphene-diamond-based nanomaterials are also convenient for the fabrication of various biosensors. Cui et al. reported on the fabrication of accurate, reliable devices for glucose detection [60]. Ni nanoparticle-modified graphene-diamond hybrid electrodes were fabricated via a catalytic thermal treatment, by which the graphene layers are directly grown on the diamond surface using Ni thin film as a catalyst. The Ni nanoparticles are formed in situ on the graphene surface due to dewetting. The interface between the Ni nanoparticles and the graphene enables efficient charge transfer during electrochemical detection. In addition, this sensor shows great selectivity, suggesting potential applications for sensitive and accurate monitoring of glucose in human blood.

L-Glutamate electrochemical sensor based on graphene and diamond was reported by Hu and co-workers [59]. The sensors were fabricated on doped chemical vapor deposition diamond electrodes and graphene nanoplatelet structures. The sensors incorporate platinum nanoparticles to catalyze the electrooxidation of hydrogen peroxide, glutamate oxidase to oxidize glutamate, and a layer of poly-phenylenediamine to convey selectivity.

Huang and co-workers reported that reduced graphene oxide and boron-doped diamond demonstrated a special impedance response regarding protein adsorption compared with other materials [58]. Besides the in-depth understanding of protein adsorption behavior, this study also indicates a potential way to control the orientations of protein molecules on a solid surface.

The electrochemical behavior of epinephrine at graphene-modified boron-doped diamond electrodes was studied by Marcu et al. [65]. It appears that the presence of the graphene layer promotes the overall oxidation process. Additional investigations carried out at different pH point out that the best sensitivity of GN/BD-diamond toward epinephrine oxidation is obtained at pH 7. Epinephrine detection in the presence of uric acid, with relevance for the detection of biological compounds, can be achieved at relatively low or high pH.

Boron-doped graphene and boron-doped diamond electrodes were also tested for the detection of various biomarkers [72]. The authors demonstrated that even though both materials exhibit similar heterogeneous electron transfer towards ferro/ferricyanide, there are dramatic differences towards the oxidation of biomolecules, such as ascorbic acid, uric acid, dopamine, and beta-nicotinamide adenine dinucleotide.

 doi:10.20944/preprints202107.0647.v1

Yuan et al. reported on the fabrication of few-layer graphene directly on a high-pressure, high temperature (HPHT) diamond substrate via sp^3-to-sp^2 conversion by catalytic thermal treatment and using diamond itself as the carbon source [73]. The hybrid electrode prototype was highly conductive and had a linear electrochemical response to dopamine. Based on the strong interfacial bonding between graphene and HPHT diamond, regeneration of the fouled electrode and full performance recovery would be easily achieved by ultrasonic cleaning.

4. Graphene – diamond interfaces and heterojunctions

The interface between the sp^2 and sp^3 nanocarbons, where the two nanoallotropes are in intimate contact, is the most exciting entity in the graphene-diamond-based nanomaterials. It ensures the two-way communication channel for the charge, spin, molecule, and phonon transport and provides the fragile stability of the carbon atoms' in the desired configuration. Thus, the interface is responsible for the graphene-diamond heterostructures' outstanding lubrication and mechanical properties; this topic will be discussed in the first part of this section. In the second part, an essential role in charge and spin transfer in emergent nanoelectronics applications will be addressed.

4.1. Friction, tribology, and mechanical properties

The achievement of the superlubricity regime is the Holy Grail of many tribological applications. For example, tribochemical reactions promoted by the oil lubrication generate structural changes in the carbon hybridization of the ta-C hydrogen-free carbon, with initially high sp^3 content. Interestingly, the macroscopic superlow friction regime of moving mechanical assemblies coated with ta-C can be attributed to a few partially oxidized graphene-like sheets, with a thickness of not more than 1 nm, formed at the surface inside the wear scar. The sp^2 planar carbon and oxygen-derived species are the hallmarks of these mesoscopic surface structures created on top of colliding asperities as a result of the tribochemical reactions induced by the oleic acid lubrication. Atomistic simulations elucidate the tribo-formation of such graphene-like structures, providing the link between the overall atomistic mechanism and the macroscopic experimental observations of green superlubricity in the investigated ta-C/oleic acid tribological systems [77].

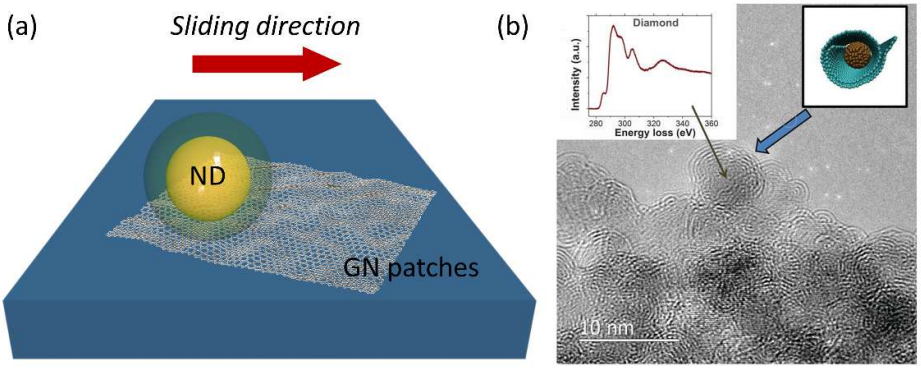

Figure 3. Superlubricity of NDs on graphene due to formation of GN@ND scrolls. (a) schematic presentation of the superlubricity test; (b) TEM image of the resulting GN@ND scrolls with the electron energy loss spectrum recorded on the ND area. Reprinted (adapted) with permission from Berman, D.; Deshmukh, S.A.; Sankaranarayanan, S.K.R.S.; Erdemir, A.; Sumant, A. V. Macroscale superlubricity enabled by graphene nanoscroll formation. Science (80) 2015, 348, 1064 1118–1122. Copyright 2015 The American Association for the Advancement of Science.

 doi:10.20944/preprints202107.0647.v1

It has been also demonstrated that using diamond brings the experimental realization of friction-free graphene one step closer [78]. Berman and his colleagues have reported a dramatic reduction in friction on the macroscale using a combination of graphene flakes and nanodiamond on a SiO_2 surface [27]. The superlubricity originates because graphene patches at a sliding interface wrap around nanodiamonds to form nanoscrolls with reduced contact area that slide against the diamond-like carbon surface, achieving an incommensurate contact and substantially reduced coefficient of friction (see Figure 3). Atomistic simulations elucidate the overall mechanism and mesoscopic link bridging the nanoscale mechanics and macroscopic experimental observations.

The extreme coefficient of friction (COF = 0.002) was recently achieved on the silicon-doped hydrogenated amorphous carbon film by lubrication with graphene oxide nanosheets in ethylene glycol [79].

The origins of low friction of hydrogenated diamond-like carbon films were investigated by Liu et al. [80]. In agreement with the work of Berman and co-workers [27], the authors concluded that the low friction occurs due to graphene nanoscroll formation depending on the sliding mode as the two-way movements in the reciprocating sliding help to keep the transfer layer within contact region, enhancing its graphitization.

Chen et al. reported on the tribological performance of as-deposited graphene – diamond films. The unique surface morphology of underneath microcrystalline film was supposed to play a crucial role in its exceptional friction performance. During the following stable sliding phase, graphene scrolls formed by graphene sheets wrapping around the wear particles they encountered and attributed to the reduction in friction by decreasing the interfacial contact area and creating an incommensurable contact between the graphene scrolls and counterpart surface [81]. The authors also reported this graphene/diamond coating friction and wear behaviors via sliding tests [82].

Enhancement on the tribological performance of diamond films by utilizing graphene coating as a solid lubricant was reported by Shen and co-workers [83]. The same collective also elucidated the atomic mechanism behind the lubricity performance of graphene-coated diamond surfaces [84]. The flexible lubrication performance of graphene on the diamond interface was also suggested by DFT calculations [85].

The lubrication behavior of hydrogenated graphene on a substrate of diamond-like carbon films was investigated via molecular dynamics simulations [86]. Hydrogenated graphene exhibits excellent lubrication behaviors at low or intermediate normal loads but loses its lubrication effect at high normal loads. In addition, it is demonstrated that the friction force is unaffected by the asperities with small periodicity around the substrate surface. Moreover, the improved lubrication for multilayer hydrogenated graphene is sensitive to its adhesion interactions with substrate, which is different from previously reported cases. Although the rigidity of hydrogenated graphene increases induced by chemical modifications, its larger friction force results from the atomic-level roughness. It is believed that these findings can provide a guideline for the superlubricity design based on the chemically modified graphene.

Also, the adhesion of a graphene monolayer onto a non-, B-, or N-doped diamond (111) surface was investigated by first-principle calculations [87,88]. The authors concluded that the graphene layer kept its aromatic character for all terminations. However, a minor charge transfer was observed from the graphene adlayer towards the non-doped and doped diamond (111) substrates.

For applications in space, the tribological properties of graphene and MWCNTs additives in diamond-like carbon/ionic liquids hybrid films in different lubricating states at high vacuum were studied by Zhang et al. [89]. The authors concluded that MWCNTs and graphene present different nano-scale tribological mechanisms and produce various lubricating effects.

The frictional properties of the interface between graphene nanoflake and single-crystalline diamond substrate have been investigated by molecular dynamics simulations

[90]. Generally, the friction coefficient was lowest when a graphene flake slid along its armchair direction and the highest when it slid along its zigzag direction.

Another aspect of the graphene-diamond interface has been addressed by Machado et al. [91]. Using molecular-dynamics simulations of tensile deformation and shear loading tests, mechanical properties of superlattices of diamond-like nanocrystals embedded in twisted bilayer graphene generated by covalent interlayer bonding through patterned hydrogenation were investigated. The authors suggested that the mechanical properties of these superstructures can be precisely tuned by controlling the fraction of sp^3-hybridized C-C bonds in the material, e.g., through the extent of chemical functionalization.

The stability, elastic moduli and deformation behavior of graphene-based diamond-like phases were also examined by molecular dynamics simulations [92]. The authors found out that the main mechanisms of non-elastic deformation is the stretching of the covalent bonds and valent angles.

An interesting problem related to the graphene-diamond lubrication properties is the frictional contact between a diamond tip and graphene edges during atomic force microscopy (AFM) experiments. Molecular dynamics simulation was used to analyze the specific changes of friction and graphene morphology with different parameters of tip shape. The results showed that the shape parameters have considerable effects on friction behavior during the tip slides on the graphene step edges [93].

4.2. Nanoelectronic and spintronic platforms

Electronic properties of graphene-single crystal diamond heterostructures attracted considerable attention due to their potential exploitation in nanoelectronics, optoelectronic, and spintronic devices. Besides the graphene-single crystal diamond heterostructures [94,95], the properties of nanocarbon hybrids were also investigated.

The electronic properties of graphene sheets decorated with nanodiamond particles have been investigated by Wang and co-workers [96]. At the ND-bonded regions, the atoms of graphene lattice follow sp^3-like bonding, and such areas play the role of conduction bottlenecks for the percolating sp^2 graphene network. The low-temperature charge transport reveals an insulating behavior for the disordered system associated with Anderson localization for the charge carriers in graphene. A large negative magnetoresistance is observed in this insulating regime, and its origin is discussed in the context of magnetic correlations of the localized charge carriers with local magnetic domains and extrinsic metal impurities associated with the ND.

Hu and co-workers prepared high mobility n-type conductive hybridized carbon films with microstructures dominantly comprising of ultrananocrystalline diamond and graphene nanoribbons via oxygen ion implantation and thermal oxidization annealing. The O^+-implanted diamond grains terminated by C=O bonds provide a conductive network surrounding diamond grains. Thus n-type Hall mobility attains high values. These hybridized carbon films can be applied in the areas of electronic devices, field emission displayers, and electrochemical electrodes [97].

Bogdanowicz and co-workers reported on the first step towards a low-temperature diamond-based transistor using thin boron-doped diamond nanosheets grown on tantalum foil substrates transferred to Si/SiO_2 and graphene [98]. The resulting device exhibits thermionic conductance and variable hopping above and below 50 K, respectively.

Interaction between graphene and the semiconducting diamond substrate has been examined with large-scale density functional theory calculations by Hu et al. [99]. No charge transfer between graphene and diamond (100) surfaces is detected, while different charge-transfer complexes are formed between graphene and diamond (111) surfaces, inducing either p-type or n-type doping on graphene. The diamond was proposed as a convenient substrate for graphene-based nanoelectronics devices. Hu et al. also applied first-principles calculation and the phonon Boltzmann transport equation to explore diffusive thermal conductivity of diamond-like bi-layer graphene (diamane, see Figure 2(a)) [100].

More complex systems - fluorinated graphene oxide, nanocrystalline diamond multilayer thin films have been proposed for optical and electromagnetic limiting applications [101].

Konabe et al. investigated the possibility of multiple exciton-generation in graphene nanostructures using tight-binding calculations [102]. They show that multiple-exciton generation occurs in graphene nanoribbons with armchair edges wherein photoelectric conversion efficiency exceeds 100%. They demonstrated that the graphene-diamond hybrid structure is a possible and robust nanostructure that can achieve multiple-exciton generation for various fast optoelectronic applications.

Atomically flat diamond-like carbon films, oabtained by the filtered cathodic vacuum arc deposition, were used as a dielectric platform for supporting graphene [103]. It was shown that graphene on these platforms had less doping from the substrate and improved FET carrier mobility compared with that of graphene on SiO_2/Si substrate. High-frequency, scaled graphene transistors on diamond-like carbon were successfully fabricated by Wu et al. [104].

Gap opening and spin injection was investigated by Ma and co-workers [105]. They addressed by first-principles calculations the electronic and magnetic properties of graphene adsorbed on the (111) surface of the diamond. They concluded that the graphene adsorbed on the diamond surface is a semiconductor with a finite gap depending on the adsorption arrangements due to the variation of on-site energy induced by the diamond surface, with the extra advantage of maintaining the main characters of the linear band dispersion of graphene. Moreover, the electronic spin can arise "intrinsically" in graphene owing to the exchange proximity interaction between electrons in graphene and localized electrons in the diamond surface rather than the characteristic graphene states. These predications make this system a viable candidate to overcome all the challenges mentioned above of graphene-based electronics.

Graphene FETs with wavelength-dependent multiple optical inputs and one electrical output in response to the charge state of NV centers in diamond have been reported by Tzeng and co-workers [106]. Negative charge state NV center in diamond serves as the gate with diamond being the gate dielectric and produces an electric field to enhance the hole concentration in the graphene channel.

Yu et al. have shown that by replacing SiO_2 with synthetic diamond, one can substantially increase the current-carrying capacity of graphene [107]. They also found that the current-carrying capacity of graphene can be improved not only on the single-crystal diamond substrates but also on an inexpensive ultrananocrystalline diamond, which can be produced in a process compatible with a conventional Si technology.

The effect of vacancies on resistance at the graphene-diamond interface was investigated by molecular dynamics simulations [108]. It was observed that the distance of the vacancy(s) from the diamond-graphene interface is a determinant of the interfacial resistance, suggesting that phonon dynamics around the vacancy contribute to reducing the interfacial barrier. Also, the change of the interfacial graphene bonds as the vacancy position is varied influences the final interfacial resistance.

A first-principles study of the structural and electronic properties of two-dimensional 2D layer/hydrogen-terminated diamond (100) heterostructures was reported by Mirabedini et al. [109]. Both the 2D layers exhibit weak van der Waals interactions and develop rippled configurations with the H-diamond (100) substrate to compensate for the induced strain. In the graphene/H-diamond (100) heterostructure, the semi-metallic characteristic of the graphene layer is preserved. On the other hand, the hBN/H-diamond (100) heterostructure shows semiconducting characteristics with an indirect bandgap of 3.55eV, where the hBN layer forms a Type-II band alignment with the H-diamond (100) surface. The authors concluded that a thin layer of hBN offers a defect-free interface with the H-diamond (100) surface and provides a layer-dependent tunability of electronic properties and band alignment for surface-doped diamond FETs.

 doi:10.20944/preprints202107.0647.v1

Muniz and co-workers presented a theoretical study on gap opening in a new class of carbon nanostructures formed due to the creation of covalent interlayer C-C bonds in hydrogenated twisted bilayer graphene (TBG) [110]. The resulting relaxed configurations consist of 2D superlattices of diamond-like nanocrystals embedded within the graphene layers. The same periodicity as that of the Moire pattern corresponds to the rotational layer stacking in TBG. The 2D diamond nanodomains resemble the cubic or the hexagonal diamond phase. The predicted band gap's value as wide as 1.2 eV increases monotonically with the increasing size of the embedded diamond nanodomain in the unit cell of the superlattice.

Selli et al. investigated the interaction of a graphene monolayer with the C(111) diamond surface using ab initio DFT and quantum transport calculations [111]. They revealed how the buckling of the graphene layer and the associated bonding to the diamond substrate affect the transport properties. They observed highly anisotropic electrical properties. The hybrid graphene-diamond system displays high carrier mobility along the ridges and a wide transport gap in the direction normal to the ridges, which qualify the system as a viable candidate for electronic nanodevices.

Shiga and co-workers theoretically investigated the electronic, magnetic, and thermal properties of a graphene-diamond hybrid structure consisting of a graphene nanoribbon with zigzag edges connected to diamond surfaces [112]. They found that the hybrid structure is stable and that the ferromagnetically ordered edge state appears. They proposed that the hybrid structure is a potential candidate for spin-polarized conducting wires with thermally efficient heat sinks.

Ueda et al. implemented graphene/diamond heterojunctions as photo-controllable memristors with photoswitchable multiple resistance states and nonvolatile memory functions [113,114]. The junctions exhibit light wavelength selectivity, and the resistance states can be switched only by blue or violet light irradiation. The mechanism for the change in photoconductivity is considered to be caused by oxidation-reduction of the graphene and/or graphene-diamond interfaces through the movement of oxygen ions by bias with photo-irradiation because they have wavelength selectivity and require air exposure for several days to exhibit memristive behavior.

Wan et al. investigated polycrystalline graphene transferred onto differently terminated epitaxial layers of boron-doped diamond [115]. Electronic interaction between the diamond and graphene was observed for n-doped graphene on the hydrogen and oxygen terminated diamond. They concluded that the wide window of achievable graphene doping is effectively determined by the diamond surface dipole, easily tuneable with varying surface functionalization. A Schottky junction using the graphene-diamond structure was clearly observed with a Schottky barrier height of 330 meV.

5. Other applications

Besides the nanoelectronics and tribology, the hybrid graphene-diamond nanomaterials appeared to be very promising for other areas of applications, such as energy storage, ultra-fast and efficient detectors, and light sources and cutting or brazing technologies. In this section, the most important cases with broad application potential will be discussed.

5.1 Energy storage - supercapacitors

Banerjee et al. presented a one-step synthesis method to produce conductive boron-doped hybrid carbon nanowalls, where sp^2-bonded graphene has been integrated with and over a three-dimensional curved wall-like network of sp^3-bonded diamond [116]. Interestingly, these hybrid graphene-diamond electrodes yield a high double-layer capacitance value of 0.43 $mF.cm^{-2}$ and electrode retention of 98% over 10 000 cycles of charging/discharging in 1 M Na_2SO_4 electrolyte. The remarkable supercapacitive performance

 doi:10.20944/preprints202107.0647.v1

was attributed to the 3D interconnected network of diamond nanowalls surrounded by highly conducting graphene.

Boron-doped graphene/boron-doped diamond was synthesized by an electron-assisted hot-filament chemical vapor deposition method, and a symmetric supercapacitor was fabricated to evaluate the practical application of the hybrid electrode. The supercapacitor delivers a high energy density and has a long-term stability advantage at high operating voltages [117].

Flexible mesoporous graphitic films with onion-like carbon nanoparticles sandwiched between thermally reduced graphene oxide (or graphene) sheets were prepared by Sun and colleagues [118], see Figure 4. The films releaved very high specific surface area (~ 420 m^2g^{-1}) due to the presence of mesopores, and they were successfully tested as the electrodes of supercapacitors without the need for the addition of a polymer binder or a conductive additive.

Composites of RGO-modified with N particles were also used as efficient electrodes in electrochemical supercapacitors [119].

3D network of graphene nanowalls on the CVD diamond film has been synthesized on the diamond by direct-current plasma-enhanced CVD on silicon substrates pre-seeded with diamond nanoparticles in gas mixtures of methane and hydrogen [120]. The system shows excellent electrochemical durability with a low background current in a wide electrochemical potential window, which makes it a promising candidate for energy storage platforms.

Nitrogen-incorporated ultrananocrystalline diamond and graphene nanowalls coated graphite, and silicon anodes were fabricated to improve the performance of anodes in lithium-ion batteries [69].

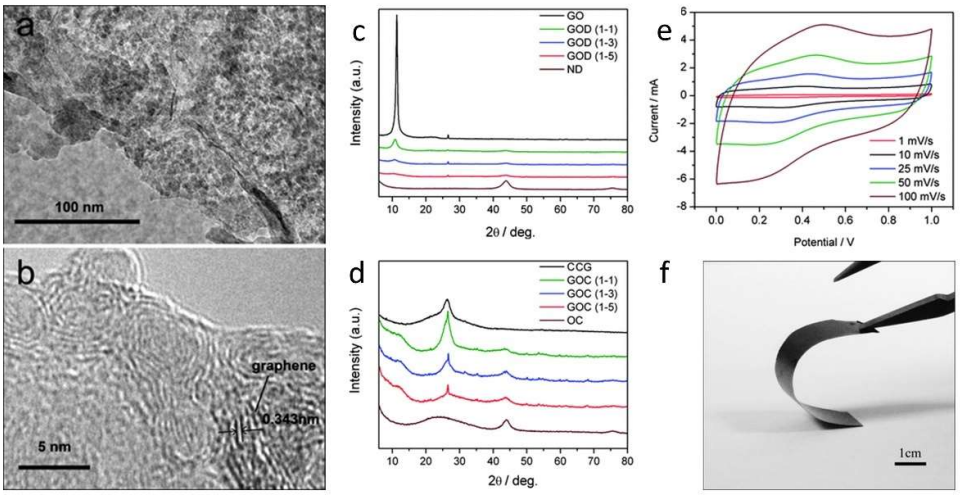

Figure 4. Example of graphene oxide – diamond composites for supercapacitors. Panels (a) and (b) present HR TEM images of the morphology at the nanoscale; panels (c) and (d) show typical XRD patterns of GO, ND particles, chemically converted GN films (CCG), onion-like carbon (OC), and mesoporous CCG/OC (GOC) composite films; panels (e) and (f) show a cyclic voltammetry and photograph of the GOC film, respectively. Reprinted (adapted) with permission from Sun, Y.Q.; Wu, Q.O.; Xu, Y.X.; Bai, H.; Li, C.; Shi, G.Q. Highly conductive and flexible mesoporous graphitic films prepared 1278 by graphitizing the composites of graphene oxide and nanodiamond. *J. Mater. Chem.* **2011**, *21*, 7154–7160. Copyright 2011 Royal Society of Chemistry.

 doi:10.20944/preprints202107.0647.v1

5.2 Detectors and light sources

A novel kind of detector based on polycrystalline grade diamond substrate and RGO contacts is reported by Benfante and co-workers [121]. This detector combines some of the good qualities of diamond with low-impedance contacts. This characteristic, together with the possibility of patterning the electrodes with standard lithographic techniques, makes this detector particularly suitable for X-ray beam monitors where the photon beam's intensity and position need to be measured with minimal effect on the beam itself.

Another application related to ultra-fast detection is converting the NV-diamond signal via coupling to graphene [122]. It has been shown that emitters, such as fluorophores and NV centers in diamond, can exhibit a strong non-radiative energy transfer to graphene, which can be read out by detecting corresponding currents with a picosecond time resolution. These results open the avenue for incorporating nitrogen-vacancy centers into ultrafast electronic circuits and electronically harvesting non-radiative transfer processes. Liu et al. suggested that the mode values of lifetime and intensity of the fluorescence from the single NV center in nanodiamond on monolayer graphene are shorter and weaker than that on bare quartz substrate [9].

For applications in diamond-based cold cathode emission devices, electron field emission (EFE) properties of ultrananocrystalline diamond films were improved by the formation of graphene nanoribbons during high-temperature annealing [97]. Also, GN/UNCD double-layer structures were reported to enhance the EFE [123]. The improvement of the plasma illumination properties and EFE due to the application of nanocrystalline diamond-decorated graphene nanoflakes, self-organized multi-layered graphene-boron-doped diamond hybrid nanowalls, and few-layer graphene-diamond nanorods hybrids were investigated thoroughly by Shankaran et al. [124–126]. They concluded that nanographitic phases in the grain boundaries of the diamond grains form electron transport networks that lead to improvement in the EFE characteristics. Free-standing graphene-diamond hybrid films for EF devices have also been fabricated using saturated hydrocarbon polymers as seeding material by hot filament chemical vapor deposition technique [127]. EFE in graphene/n-type diamond heterojunctions was also investigated by Yamada et al. [128,129].

Santos and co-workers also reported that the morpho-structural aspects are critical regarding the EFE behavior of graphene-diamond hybrids [130]. They suggested emission from both the background graphene and the protruded NCD clusters.

Interface engineering of a silicon/graphene heterojunction photodetector via a diamond-like carbon interlayer was suggested by Yang and co-workers [131]. The heterojunction can simultaneously exhibit improved photoresponsivity and response speed compared with the counterparts without DLC interlayers. The authors also concluded that incorporation of the DLC interlayer might be a universal strategy to construct hybrid interfaces with high performance in next-generation optoelectronic devices.

Huang et al. constructed ultraviolet photodetectors based on ultra-nanocrystalline diamond and dispersed graphene flakes with ZnO nanotubes [132], see Figure 5. The distribution of graphene and nanodiamonds interlayer enables the new energy levels on the conduction band, which reduces the barrier height to allow fast charge carrier transportation during the UV illumination. It is believed that their addition increases the UV adsorptivity and sufficient amount of conducting path within ZnO nanotubes. Therefore, the present photodetector can be used as an efficient UV photodetection device with high performance and opening up new opportunities for future optoelectronic devices.

Another type of UV detector based on the heterojunction between graphene and microcrystalline diamond was demonstrated by Wei et al. [133]. A vertical graphene/MCD/metal structure is constructed as the photodiode device using graphene as the transparent top electrode for solar-blind UV sensing with high responsivity and gain factor. Also, Yao et al. reported on a graphene-diamond-metal thin-film system as a UV light sensor on a flexible substrate [134].

Preprints (www.preprints.org) | NOT PEER-REVIEWED | Posted: 29 July 2021 doi:10.20944/preprints202107.0647.v1

Weinhold and co-workers demonstrated optoelectronic function in a near-to-monolayer molecular architecture approaching atomically defined spatial disposition of all components [135]. The active layer consisted of a self-assembled terylene-based dye, forming a bicomponent supramolecular network with melamine. The assembly at the graphene-diamond interface shows an absorption maximum at 740 nm whereby the photoresponse was measured with a gallium counter electrode.

Zhang et al. reported on fabrication of the RGO/Au electrode on (111)-oriented polycrystalline diamond films on Si substrates for alpha particles detectors [136]. The dark current, photocurrent, and energy resolution of these detectors under 5.5 MeV alpha particles irradiation from an Am-241 source were observed. The results demonstrated that fabrication of the RGO/Au electrode on PCD might provide a feasible way to improve its detection performance under alpha particles irradiation.

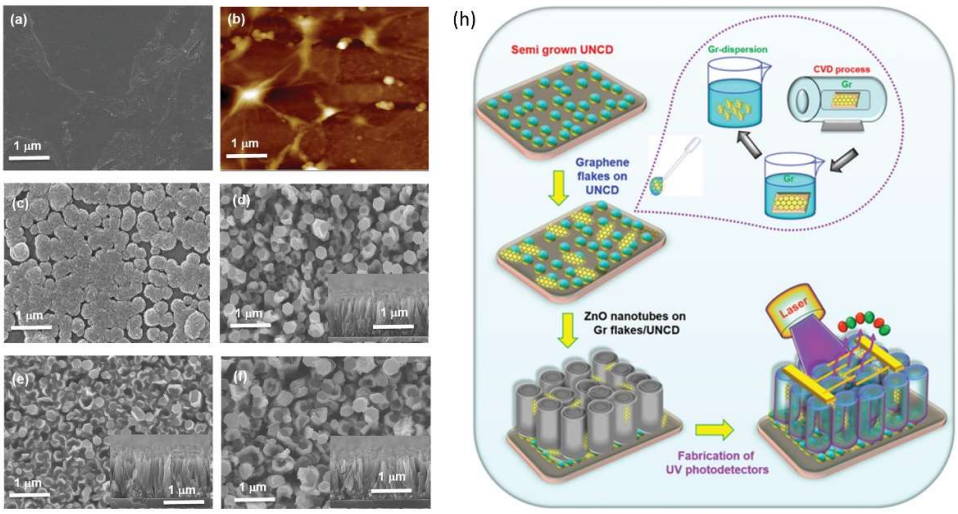

Figure 5. High-performance photodetector based on graphene flakes, UNCD and ZnO nanotubes. (a) FESEM image of graphene layer, (b) AFM image of graphene layer, and (c) FESEM images of semigrown UNCD materials grown for 5 min. (d)–(f) FESEM images of UNCD-ZNT, GrF-ZnTs, and GrF-ZnTs/UNCD heterostructures. (h) Fabrication flow diagram of the UV photodetector. Reprinted (adapted) with permission from Huang, B.R.; Saravanan, A.; Lu, H.C. Structural Engineering of Dispersed Graphene Flakes into ZnO Nanotubes on 1316 Discontinues Ultra-Nanocrystalline Diamond Substrates for High-Performance Photodetector with Excellent UV Light to 1317 Dark Current Ratios. *Adv. Mater. INTERFACES* **2020**, *7*, doi:10.1002/admi.201901694. Copyright 2020 Jonh Willey and Sons.

5.3 Materials' processing technologies

The graphene-diamond materials are also important in materials' processing. For example, graphene, GO, and RGO attracted attention in cutting technologies. For example, the addition of graphene also improves the performance of polycrystalline diamond compact (PDC) [137]. A new type of high-performance diamond composite PDC-G was prepared and compared with PDC without graphene; the hardness and wear resistance of PDC-G with 0.1 wt% graphene addition were enhanced by 75% and 33%, respectively. Moreover, the electrical conductivity of PDC prepared by graphene strengthening was improved 42-fold. The strengthening mechanism of PDC-G mainly occurred as a result of the lubricating effect of graphene between diamond particles. Graphene pallets are very efficient in suppressing the chemical wear of the tool in diamond cutting [138].

GO was also used to improve the wear resistance and service life of the epoxy resin-bonded diamond abrasive tools [139].

 doi:10.20944/preprints202107.0647.v1

On the other hand, multilayer graphene can help to reduce unfavorable thermal damage of diamonds in the current brazing practice [140,141]. It has also been reported that colloidal suspensions of graphene oxide mitigate carbon diffusion during diamond turning of steel [142].

Also, the rheology of mixed nanocarbon dispersions attracted some attention. For example, Ilyas et al. addressed the use of graphene-diamond materials in thermo-fluid technologies [143]. They investigated the rheological behavior of hybrid nanosuspensions containing high thermally conductive diamond and graphene nanoplatelets (1:1) and supported their results with extensive machine learning methods to predict the viscosity of hybrid nanofluids based on the three input parameters (temperature, concentration, and shear rate).

Jiang et al. investigated epoxy composites of graphene and nanodiamond [144]. They developed a single-step process to cast epoxy composites with high thermal conductivity and low electric conductivity. They found that the graphene coating improves the dispersion of diamond in the polymer matrix. It also decreases the interfacial thermal resistance between the diamond and epoxy while preserving excellent electrical insulation.

Epoxy thin film composites filled with particulate nanofillers; synthetic diamond and graphene nanoplatelets were studied by Saw et al. [145]. The influences of these two types of fillers, especially in terms of their loading, sizes, and shapes, were discussed. It was found that the epoxy thin-film composites incorporating synthetic diamond displayed optimum properties where the addition of synthetic diamond from 0 to 2 vol.% results in higher elastic modulus, tensile strength, elongation at break, thermal conductivity, and storage modulus than graphene nanoplatelet composites. Both thin-film composites showed improvement in the glass transition temperature with increasing filler loadings. Results on the electrical conductivity of both systems showed that higher conductivity is observed in graphene nanoplatelets composites if compared to synthetic diamond composites.

Bittencourt et al. carried out a numerical simulation yielding the size distribution of graphene clusters as a filler of a polymer aiming to obtain the percolation threshold [146]. The probability density of this distribution shows a universal complementary Fermi-Dirac behavior as a sign of a topological response. Using a tight-binding model for the transmission from the source to the drain, they obtain a smooth transition from an insulator to a conductor through a dirty metal as the concentration of conductive bonds increases for small arrays. As the array size increases, the simulation shows a sharp non-metal-to-metal transition from a pure polymer into a pristine suspended graphene layer

A new thermal conductive poly(vinylidene fluoride) composite has been developed via a hybrid functionalized graphene sheets - nanodiamonds filler by a simple solution method. The composite showed different thermal conductivities at different proportions of hybrid filler [147].

Shul'zhenko and co-workers developed a process for the uniform distribution of n-layer graphenes in a mixture for sintering polycrystalline diamond at high pressures and temperatures, providing current-conducting diamond polycrystals [148].

The GO was found to improve the growth rate of CVD diamond coating by increasing the chemical reaction rate [149]. A novel method of dispersing GO particles as adsorbent on the substrate prior to deposition was proposed, with which the diamond coating with large grain size and high thickness was deposited on the silicon nitride under the normal CVD environment.

Interestingly, nitrogen-incorporated ultrananocrystalline diamond and multi-layer-graphene-like hybrid carbon films were employed in the construction of biocompatible carbon-based heaters for possible electrosurgical applications [150].

The diamond and graphene also met on the way to scale up for industrial production of GO. A combination of fused-deposition-modeling-based 3D printing and highly robust BD-diamond with a wide electrochemical potential window allowed to fabricate a scala-

 doi:10.20944/preprints202107.0647.v1

ble packed-bed electrochemical reactor for GO production [151]. The scalability of the reactor along the vertical and lateral dimensions was systematically demonstrated to facilitate its eventual industrial application, capable of producing electrochemically derived GO on a multiple-gram scale.

5.4. Catalysis

Graphene-diamond nanomaterials also serve as efficient catalysts or catalyst carriers. Lan et al. suggested the use of graphene-diamond nanomaterials for catalytic applications [152]. A defective nanodiamond-graphene material exhibits superior catalytic activity in acetylene hydrochlorination with an acetylene conversion of 50%, selectivity to vinyl chloride of up to 99.5%. It is the first example of a metal-free catalyst with comparable performance to that of the 0.25% Au/C catalyst.

Graphene aerogels and graphene aerogel-nanodiamond hybrids have been fabricated by a mild reduction/self-assembly hydrothermal method using graphene oxide dispersion as a precursor [153]. The aerogels have been used as metal-free catalysts for oxidative dehydrogenation of propane. Reduced graphene oxide aerogels without nanodiamonds outperformed carbon nanotubes in propene productivity and selectivity, correlated with a higher content of accessible carbonyl-quinone groups and more defective structures of reduced graphene oxide. Graphene aerogels loaded with low amounts of nanodiamonds (2 wt%) by a one-pot strategy provided 18% higher activity than RGO aerogels, ascribed to the increase of the sp^3/sp^2 ratio. Hybrid aerogels are freestanding, robust, and highly porous monoliths, which is a suitable platform for catalysts or adsorbents in flow systems.

A core/shell structure nanodiamond/graphene (ND/G) was prepared by annealing ND in a vacuum at temperatures of 1200 and 1500 °C. The prepared ND/G was used as a support for a platinum electrocatalyst in direct methanol fuel cells. Higher dispersion of Pt nanoparticles was observed on ND/G compared to pristine NDs, and the material showed better catalytic activity and greater stability for methanol electro-oxidation than Pt/ND [154].

5.5. Generation of extreme environments

Graphene and diamond were also suggested in several exotic applications. For example, water molecules can be confined in nanobubbles at the hybrid interfaces of graphene and diamond surfaces at varying temperatures [155]. A molecular dynamics simulation revealed that the molecules confined in small nanobubbles at high density are found to possess very slow relaxation time scales because of stronger hydrogen bonding and spatial constraints. These water molecules can be considered as essentially irrotational. In other cases, water molecules confined in nanobubbles at a lower density at supercritical temperature are found to show very fast relaxation time scales as the thermal energy dominates the dynamics of water molecules in these cases.

Lim and co-workers exploited the hardness and virtual incompressibility of diamond to be used in miniature high-pressure anvil cells [156]. They reported on a new way to generate static pressure by encapsulating single-crystal diamond with graphene membrane. Heating the diamond-graphene interface to the reconstruction temperature of diamond produces a high density of graphene nanobubbles that can also trap water. At high temperatures, chemical bonding between graphene and diamond is robust enough to allow the hybrid interface to act as a hydrothermal anvil cell due to the impermeability of graphene. Superheated water trapped within the pressurized graphene nanobubbles is observed to etch the diamond surface to produce a high density of square-shaped voids.

6. Summary and outlooks

Graphene-diamond nanomaterials, heterojunctions, and derived hybrid nanosystems are an important class of all-carbon materials. The common denominators of the vast

 doi:10.20944/preprints202107.0647.v1

majority of technological and fundamental issues are the successful implementation of two-way communication between the graphene and diamond and the fragile interplay between the two border arrangements given by the sp^2 and sp^3 hybridization of the carbon atoms. Rational design and directed modification of the nanointerface and the implementation of functional nano links thus represent the major challenge in further developing graphene-diamond-based nanomaterials and devices. Correspondingly, engineering the interface demonstrates an interesting topological problem - a reorganization can occur at partial atomic structures or in terms of topographic modulation.

As can be seen even from the concise review, both sp^2 and sp^3 carbon allotropes offer many opportunities, especially when approaching the nanoscale dimensions, and many physical and chemical properties have already been utilized in practice. Note that the environment, which hides many pitfalls for implementing these nano-sized compounds into functional devices, should their exceptional properties not be compromised. Consequently, a next step - the bilateral communication of the nanocarbons and the surroundings, through highly efficient channels - the interfaces and the covalent links - must be promoted and rationalized in the near future.

Abbreviations:

0D, 1D, 2D, 3D – zero-, one-, two-, three-dimensional

AFM – atomic force microscopy

BD – boron-doped, e.g., BDND – boron-doped nanodiamond

CVD – chemical vapor deposition

DFT – density functional theory

EDCL - electrochemical double-layer capacitance

EFE – electron field emission

FET – field-effect transistor

GC – glassy carbon

GO – graphene oxide

GN – graphene

HPHT – high-pressure high-temperature

HR TEM – high-resolution transmission electron microscopy

MCD – microcrystalline diamond

ML – multi-layer, e.g., MLGN – multi-layer graphene

ND – nanodiamond

NV – nitrogen-vacancy

ORR – oxygen reduced reaction

PCD – polycrystalline diamond compact

RGO – reduced graphene oxide

TBG – twisted bilayer graphene

UNCD - ultra-nanocrystalline diamond

UV – ultraviolet

XRD – X-ray diffraction

Author Contributions: methodology, J.V.; writing—original draft preparation, J.V.; writing—review and editing, J.V.; visualization, J.V.; supervision, J.V.; project administration, J.V.; funding acquisition, J.V. All authors have read and agreed to the published version of the manuscript.

Funding: This research was funded by the Ministry of Education, Youth and Sports of the Czech Republic under Operational Programme Research, Development and Education, project Carbon allotropes with rationalized nanointerfaces and nanolinks for environmental and biomedical applications (CARAT), number CZ.02.1.01/0.0/0.0/16_026/0008382.

Conflicts of Interest: The authors declare no conflict of interest.

References

1. Allen, M.J.; Tung, V.C.; Kaner, R.B. Honeycomb Carbon: A Review of Graphene. *Chem. Rev.* **2010**, *110*, 132–145, doi:10.1021/cr900070d.
2. El-Kady, M.F.; Shao, Y.; Kaner, R.B. Graphene for batteries, supercapacitors and beyond. *Nat. Rev. Mater.* **2016**, *1*, 16033, doi:10.1038/natrevmats.2016.33.
3. Nag, A.; Mitra, A.; Mukhopadhyay, S.C. Graphene and its sensor-based applications: A review. *Sensors Actuators, A Phys.* **2018**, *270*, 177–194, doi:10.1016/j.sna.2017.12.028.
4. Ahn, E.C. 2D materials for spintronic devices. *npj 2D Mater. Appl.* **2020**, *4*, doi:10.1038/s41699-020-0152-0.
5. Kang, S.; Lee, D.; Kim, J.; Capasso, A.; Kang, H.S.; Park, J.W.; Lee, C.H.; Lee, G.H. 2D semiconducting materials for electronic and optoelectronic applications: Potential and challenge. *2D Mater.* **2020**, *7*, doi:10.1088/2053-1583/ab6267.
6. Yu. Dolmatov, V. Detonation synthesis ultradispersed diamonds: properties and applications. *Russ. Chem. Rev.* **2001**, *70*, 607–626, doi:10.1070/RC2001v070n07ABEH000665.
7. Nunn, N.; Torelli, M.; McGuire, G.; Shenderova, O. Nanodiamond: A high impact nanomaterial. *Curr. Opin. Solid State Mater. Sci.* **2017**, *21*, 1–9, doi:https://doi.org/10.1016/j.cossms.2016.06.008.
8. Shenderova, O.A.; McGuire, G.E. Science and engineering of nanodiamond particle surfaces for biological applications (Review). *Biointerphases* **2015**, *10*, 30802, doi:10.1116/1.4927679.
9. Liu, X.D.; Wang, G.Z.; Song, X.R.; Feng, F.P.; Zhu, W.; Lou, L.R.; Wang, J.F.; Wang, H.; Bao, P.F. Energy transfer from a single nitrogen-vacancy center in nanodiamond to a graphene monolayer. *Appl. Phys. Lett.* **2012**, *101*, doi:10.1063/1.4769367.
10. Bray, K.; Cheung, L.; Hossain, K.R.; Aharonovich, I.; Valenzuela, S.M.; Shimoni, O. Versatile multicolor nanodiamond probes for intracellular imaging and targeted labeling. *J. Mater. Chem. B* **2018**, *6*, 3078–3084, doi:10.1039/c8tb00508g.
11. Rondin, L.; Tetienne, J.-P.; Hingant, T.; Roch, J.-F.; Maletinsky, P.; Jacques, V. Magnetometry with nitrogen-vacancy defects in diamond. *Reports Prog. Phys.* **2014**, *77*, 056503, doi:10.1088/0034-4885/77/5/056503.
12. Alekseev, N.I. Matrix Synthesis of Graphene on a Diamond Surface and Its Simulation. *Russ. J. Phys. Chem. A* **2018**, *92*, 1369–1374, doi:10.1134/S0036024418070038.
13. Kvashnin, A.G.; Chernozatonskii, L.A.; Yakobson, B.I.; Sorokin, P.B. Phase Diagram of Quasi-Two-Dimensional Carbon, From Graphene to Diamond. *NANO Lett.* **2014**, *14*, 676–681, doi:10.1021/nl403938g.
14. Antipina, L.Y.; Sorokin, P.B. Converting Chemically Functionalized Few-Layer Graphene to Diamond Films: A Computational Study. *J. Phys. Chem. C* **2015**, *119*, 2828–2836, doi:10.1021/jp510390b.
15. Belenkov, E.A.; Greshnyakov, V.A. Diamond-like phases prepared from graphene layers. *Phys. SOLID STATE* **2015**, *57*, 205–212, doi:10.1134/S1063783415010047.
16. Geng, P.; Branicio, P.S. Atomistic insights on the pressure-induced multi-layer graphene to diamond-like structure transformation. *Carbon N. Y.* **2021**, *175*, 243–253, doi:10.1016/j.carbon.2021.01.007.
17. Xu, M.J.; Zhang, Y.Z.; Zhang, J.; Lu, J.Y.; Qian, B.J.; Lu, D.J.; Zhang, Y.F.; Wang, L.; Chen, X.S.; Shigekawa, H. Spontaneous formation of graphene-like stripes on high-index diamond C(331) surface. *NANOSCALE Res. Lett.* **2012**, *7*, doi:10.1186/1556-276X-7-460.
18. van Wijk, M.M.; Fasolino, A. Minimal graphene thickness for wear protection of diamond. *AIP Adv.* **2015**, *5*, doi:10.1063/1.4905942.
19. Cellini, F.; Lavini, F.; Cao, T.F.; de Heer, W.; Berger, C.; Bongiorno, A.; Riedo, E. Epitaxial two-layer graphene under pressure: Diamene stiffer than Diamond. *FLATCHEM* **2018**, *10*, 8–13, doi:10.1016/j.flatc.2018.08.001.
20. Erohin, S. V; Ruan, Q.Y.; Sorokin, P.B.; Yakobson, B.I. Nano-Thermodynamics of Chemically Induced Graphene-Diamond Transformation. *SMALL* **2020**, *16*, doi:10.1002/smll.202004782.
21. Paul, S.; Momeni, K. Mechanochemistry of Stable Diamane and Atomically Thin Diamond Films Synthesis from Bi- and Multilayer Graphene: A Computational Study. *J. Phys. Chem. C* **2019**, *123*, 15751–15760, doi:10.1021/acs.jpcc.9b02149.
22. Bakharev, P. V; Huang, M.; Saxena, M.; Lee, S.W.; Joo, S.H.; Park, S.O.; Dong, J.C.; Camacho-Mojica, D.C.; Jin, S.; Kwon, Y.; et al. Chemically induced transformation of chemical vapour deposition grown bilayer graphene into fluorinated single-layer diamond. *Nat. Nanotechnol.* **2020**, *15*, 59-+, doi:10.1038/s41565-019-0582-z.
23. Ke, F.; Zhang, L.; Chen, Y.; Yin, K.; Wang, C.; Tzeng, Y.K.; Lin, Y.; Dong, H.; Liu, Z.; Tse, J.S.; et al. Synthesis of Atomically Thin Hexagonal Diamond with Compression. *Nano Lett.* **2020**, *20*, 5916–5921, doi:10.1021/acs.nanolett.0c01872.
24. Greshnyakov, V.A.; Belenkov, E.A. Structure and properties of diamond-like phase obtained from tetragonal graphene layers. *Lett. Mater. MA O Mater.* **2016**, *6*, 159–162, doi:10.22226/2410-3535-2016-3-159-162.

25. Bai, S.D.; Xu, J.X.; Wang, Y.; Zhang, Q.; Tsuruda, T.; Higuchi, Y.; Ozawa, N.; Adachi, K.; Martin, J.M.; Kubo, M. Generation of "Graphene Arch-Bridge" on a Diamond Surface by Si Doping: A First-Principles Computational Study. *J. Phys. Chem. C* **2020**, *124*, 26379–26386, doi:10.1021/acs.jpcc.0c09716.
26. Nemeth, P.; McColl, K.; Smith, R.L.; Murri, M.; Garvie, L.A.J.; Alvaro, M.; Pecz, B.; Jones, A.P.; Cora, F.; Salzmann, C.G.; et al. Diamond-Graphene Composite Nanostructures. *NANO Lett.* **2020**, *20*, 3611–3619, doi:10.1021/acs.nanolett.0c00556.
27. Berman, D.; Deshmukh, S.A.; Sankaranarayanan, S.K.R.S.; Erdemir, A.; Sumant, A. V. Macroscale superlubricity enabled by graphene nanoscroll formation. *Science.* **2015**, *348*, 1118–1122, doi:10.1126/science.1262024.
28. Radosinski, L.; Formalik, F.; Olejniczak, A.; Radosz, A. Diaphite, a new type of surface with mixed sp 2 -sp 3 hybridization for adsorption and functionalization. *Appl. Surf. Sci.* **2017**, *404*, 154–161, doi:10.1016/j.apsusc.2017.01.085.
29. Gu, C.Z.; Li, W.X.; Xu, J.; Xu, S.C.; Lu, C.; Xu, L.F.; Li, J.J.; Zhang, S.B. Graphene grown out of diamond. *Appl. Phys. Lett.* **2016**, *109*, doi:10.1063/1.4964710.
30. Lu, C.; Yang, H.X.; Xu, J.; Xu, L.F.; Chshiev, M.; Zhang, S.B.; Gu, C.Z. Spontaneous formation of graphene on diamond (111) driven by B- doping induced surface reconstruction. *Carbon N. Y.* **2017**, *115*, 388–393, doi:10.1016/j.carbon.2017.01.030.
31. Okada, S. Formation of graphene nanostructures on diamond nanowire surfaces. *Chem. Phys. Lett.* **2009**, *483*, 128–132, doi:10.1016/j.cplett.2009.10.071.
32. Ileri, N.; Goldman, N. Graphene and nano-diamond synthesis in expansions of molten liquid carbon. *J. Chem. Phys.* **2014**, *141*, doi:10.1063/1.4899071.
33. Liu, J.; Muinos, H. V; Nordlund, K.; Djurabekova, F. Structural properties of protective diamond-like-carbon thin films grown on multilayer graphene. *J. PHYSICS-CONDENSED MATTER* **2019**, *31*, doi:10.1088/1361-648X/ab4094.
34. Carvalho, A.F.; Holz, T.; Santos, N.F.; Ferro, M.C.; Martins, M.A.; Fernandes, A.J.S.; Silva, R.F.; Costa, F.M. Simultaneous CVD synthesis of graphene-diamond hybrid films. *Carbon N. Y.* **2016**, *98*, 99–105, doi:10.1016/j.carbon.2015.10.095.
35. Ueda, K.; Aichi, S.; Asano, H. Direct formation of graphene layers on diamond by high-temperature annealing with a Cu catalyst. *Diam. Relat. Mater.* **2016**, *63*, 148–152, doi:10.1016/j.diamond.2015.10.021.
36. Cooil, S.P.; Song, F.; Williams, G.T.; Roberts, O.R.; Langstaff, D.P.; Jorgensen, B.; Hoydalsvik, K.; Breiby, D.W.; Wahlstrom, E.; Evans, D.A.; et al. Iron-mediated growth of epitaxial graphene on SiC and diamond. *Carbon N. Y.* **2012**, *50*, 5099–5105, doi:10.1016/j.carbon.2012.06.050.
37. Cooil, S.P.; Wells, J.W.; Hu, D.; Niu, Y.R.; Zakharov, A.A.; Bianchi, M.; Evans, D.A. Controlling the growth of epitaxial graphene on metalized diamond (111) surface. *Appl. Phys. Lett.* **2015**, *107*, doi:10.1063/1.4935073.
38. Garcia, J.M.; He, R.; Jiang, M.P.; Kim, P.; Pfeiffer, L.N.; Pinczuk, A. Multi layer graphene grown by precipitation upon cooling of nickel on diamond. *Carbon N. Y.* **2011**, *49*, 1006–1012, doi:10.1016/j.carbon.2010.11.008.
39. Kanada, S.; Nagai, M.; Ito, S.; Matsumoto, T.; Ogura, M.; Takeuchi, D.; Yamasaki, S.; Inokuma, T.; Tokuda, N. Fabrication of graphene on atomically flat diamond (111) surfaces using nickel as a catalyst. *Diam. Relat. Mater.* **2017**, *75*, 105–109, doi:10.1016/j.diamond.2017.02.014.
40. Berman, D.; Deshmukh, S.A.; Narayanan, B.; Sankaranarayanan, S.; Yan, Z.; Balandin, A.A.; Zinovev, A.; Rosenmann, D.; Sumant, A. V Metal-induced rapid transformation of diamond into single and multilayer graphene on wafer scale. *Nat. Commun.* **2016**, *7*, doi:10.1038/ncomms12099.
41. Rey, S.; Le Normand, F. Surface transformations of carbon (graphene, graphite, diamond, carbide), deposited on polycrystalline nickel by hot filaments chemical vapour deposition. *Thin Solid Films* **2011**, *519*, 4426–4428, doi:10.1016/j.tsf.2011.01.331.
42. Tsubota, T.; Morioka, A.; Osoekawa, Y.; Nakao, M. Direct Synthesis of Graphene Layer Covered Micro Channel on Diamond Surface Using Ni Wire. *J. Nanosci. Nanotechnol.* **2018**, *18*, 4418–4422, doi:10.1166/jnn.2018.15024.
43. Zou, H.H.; Bai, H.; Yu, J.H.; Wang, Y.; Liao, Q.L.; Nishimura, K.; Zeng, L.M.; Jiang, N. Architecting graphene nanowalls on diamond powder surface. *Compos. PART B-ENGINEERING* **2015**, *73*, 57–60, doi:10.1016/j.compositesb.2014.12.007.
44. Dai, W.; Yu, J.H.; Wang, Y.; Song, Y.Z.; Bai, H.; Jiang, N. Single crystalline 3C-SiC nanowires grown on the diamond surface with the assistance of graphene. *J. Cryst. Growth* **2015**, *420*, 6–10, doi:10.1016/j.jcrysgro.2015.03.012.
45. Li, D.S.; Zou, W.; Jiang, W.G.; Peng, X.Y.; Song, S.L.; Qin, Q.H.; Xue, J.M. Quasi homoepitaxial growth of modified diamond: Nickel-substrate catalytic multilayer graphene transforming to diamond. *Ceram. Int.* **2020**, *46*, 10885–10892, doi:10.1016/j.ceramint.2020.01.102.
46. Hussain, H.A.; Akman, N.; Ozdogan, C. Investigation of the mono vacancy effects on the structural, electronic and magnetic properties of graphene hexagonal-boron nitride in-plane hybrid embracing diamond shaped graphene island. *SOLID STATE Sci.* **2020**, *108*, doi:10.1016/j.solidstatesciences.2020.106395.
47. Zkria, A.; Haque, A.; Egiza, M.; Abubakr, E.; Murasawa, K.; Yoshitake, T.; Narayan, J. Laser-induced structure transition of diamond-like carbon coated on cemented carbide and formation of reduced graphene oxide. *MRS Commun.* **2019**, *9*, 910–915, doi:10.1557/mrc.2019.88.
48. Hembram, K.; Lee, S.; Im, H.; Ju, H.; Jeong, S.H.; Lee, J.K. The surface hybridization of diamond with vertical graphene: a new route to diamond electronics. *Mater. HORIZONS* **2020**, *7*, 470–476, doi:10.1039/c9mh01588d.
49. Zhu, L.Y.; Yao, M.G.; Dong, J.J.; Hu, K.; Liu, R.; Gong, C.; Wang, Y.; Liu, B.B. Direct Conversion of Graphene Aerogel into

Low-Density Diamond Aerogel Composed of Ultrasmall Nanocrystals. *J. Phys. Chem. C* **2018**, *122*, 13193–13198, doi:10.1021/acs.jpcc.8b03809.

50. Filonenko, V.P.; Zibrov, I.P.; Davydov, V.A.; Trenikhin, M. V PHASE FORMATION IN B-C-N SYSTEM AT HIGH PRESSURES: STRUCTURE AND CHARACTERISTICS OF HETERO-GRAPHENE AND HETERO-DIAMOND PARTICLES. *Izv. Vyss. UCHEBNYKH Zaved. KHIMIYA I KHIMICHESKAYA TEKHNOLOGIYA* **2015**, *58*, 37-+.
51. Fukuda, M.; Islam, M.S.; Sekine, Y.; Shinmei, T.; Lindoy, L.F.; Hayami, S. Crystallization of Diamond from Graphene Oxide Nanosheets by a High Temperature and High Pressure Method. *CHEMISTRYSELECT* **2021**, *6*, 3399–3402, doi:10.1002/slct.202100574.
52. Ogawa, S.; Yamada, T.; Ishizduka, S.; Yoshigoe, A.; Hasegawa, M.; Teraoka, Y.; Takakuwa, Y. Vacuum Annealing Formation of Graphene on Diamond C(111) Surfaces Studied by Real-Time Photoelectron Spectroscopy. *Jpn. J. Appl. Phys.* **2012**, *51*, doi:10.1143/JJAP.51.11PF02.
53. Tokuda, N.; Fukui, M.; Makino, T.; Takeuchi, D.; Yamsaki, S.; Inokuma, T. Formation of Graphene-on-Diamond Structure by Graphitization of Atomically Flat Diamond (111) Surface. *Jpn. J. Appl. Phys.* **2013**, *52*, doi:10.7567/JJAP.52.110121.
54. Zhao, F.; Afandi, A.; Jackman, R.B. Graphene diamond-like carbon films heterostructure. *Appl. Phys. Lett.* **2015**, *106*, doi:10.1063/1.4914495.
55. Tzeng, Y.H.; Chang, C.C. Graphene Induced Diamond Nucleation on Tungsten. *IEEE OPEN J. Nanotechnol.* **2020**, *1*, 117–127, doi:10.1109/OJNANO.2020.3038055.
56. Tinchev, S.S. Surface modification of diamond-like carbon films to graphene under low energy ion beam irradiation. *Appl. Surf. Sci.* **2012**, *258*, 2931–2934, doi:10.1016/j.apsusc.2011.11.009.
57. Tinchev, S.; Valcheva, E.; Petrova, E. Low temperature crystallization of diamond-like carbon films to graphene. *Appl. Surf. Sci.* **2013**, *280*, 512–517, doi:10.1016/j.apsusc.2013.05.019.
58. Huang, Y.X.; Hara, A.; Terashima, C.; Fujishima, A.; Takai, M. Protein adsorption behavior on reduced graphene oxide and boron-doped diamond investigated by electrochemical impedance spectroscopy. *Carbon N. Y.* **2019**, *152*, 354–362, doi:10.1016/j.carbon.2019.06.023.
59. Hu, J.P.; Wisetsuwannaphum, S.; Foord, J.S. Glutamate biosensors based on diamond and graphene platforms. *FARADAY Discuss.* **2014**, *172*, 457–472, doi:10.1039/c4fd00032c.
60. Cui, N.Y.; Guo, P.; Yuan, Q.L.; Ye, C.; Yang, M.Y.; Yang, M.H.; Chee, K.W.A.; Wang, F.; Fu, L.; Wei, Q.P.; et al. Single-Step Formation of Ni Nanoparticle-Modified Graphene-Diamond Hybrid Electrodes for Electrochemical Glucose Detection. *SENSORS* **2019**, *19*, doi:10.3390/s19132979.
61. Liu, A.P.; Xu, T.; Ren, Q.H.; Yuan, M.; Dong, W.J.; Tang, W.H. Graphene modulated 2D assembly of plasmonic gold nanostructure on diamond-like carbon substrate for surface-enhanced Raman scattering. *Electrochem. commun.* **2012**, *25*, 74–78, doi:10.1016/j.elecom.2012.09.027.
62. Jiang, M.Y.; Zhang, Z.Q.; Chen, C.K.; Ma, W.C.; Han, S.J.; Li, X.; Lu, S.H.; Hu, X.J. High efficient oxygen reduced reaction electrodes by constructing vertical graphene sheets on separated papillary granules formed nanocrystalline diamond films. *Carbon N. Y.* **2020**, *168*, 536–545, doi:10.1016/j.carbon.2020.06.031.
63. Dettlaff, A.; Jakobczyk, P.; Ficek, M.; Wilk, B.; Szal, M.; Wojta, J.; Ossowski, T.; Bogdanowicz, R. Electrochemical determination of nitroaromatic explosives at boron-doped diamond/graphene nanowall electrodes: 2,4,6-trinitrotoluene and 2,4,6-trinitroanisole in liquid effluents. *J. Hazard. Mater.* **2020**, *387*, doi:10.1016/j.jhazmat.2019.121672.
64. Gao, J.Y.; Zhang, H.Y.; Ye, C.; Yuan, Q.L.; Chee, K.W.A.; Su, W.T.; Yu, A.M.; Yu, J.H.; Lin, C.T.; Dai, D.; et al. Electrochemical Enantiomer Recognition Based on sp(3)-to-sp(2) Converted Regenerative Graphene/Diamond Electrode. *NANOMATERIALS* **2018**, *8*, doi:10.3390/nano8121050.
65. Marcu, M.; Spataru, T.; Calderon-Moreno, J.M.; Osiceanu, P.; Preda, L.; Spataru, N. Anodic Voltammetry of Epinephrine at Graphene-Modified Conductive Diamond Electrodes and Its Analytical Application. *J. Electrochem. Soc.* **2018**, *165*, B523–B529, doi:10.1149/2.1321811jes.
66. Negrea, S.; Diaconu, L.A.; Nicorescu, V.; Motoc, S.; Orha, C.; Manea, F. Graphene Oxide Electroreduced onto Boron-Doped Diamond and Electrodecorated with Silver (Ag/GO/BDD) Electrode for Tetracycline Detection in Aqueous Solution. *NANOMATERIALS* **2021**, *11*, doi:10.3390/nano11061566.
67. Pei, J.X.; Yu, X.; Zhang, Z.Q.; Zhang, J.; Wei, S.B.; Boukherroub, R. In-situ graphene modified self-supported boron-doped diamond electrode for Pb(II) electrochemical detection in seawater. *Appl. Surf. Sci.* **2020**, *527*, doi:10.1016/j.apsusc.2020.146761.
68. Peleyeju, M.G.; Idris, A.O.; Umukoro, E.H.; Babalola, J.O.; Arotiba, O.A. Electrochemical Detection of 2,4-Dichlorophenol on a Ternary Composite Electrode of Diamond, Graphene, and Polyaniline. *CHEMELECTROCHEM* **2017**, *4*, 1074–1080, doi:10.1002/celc.201600621.
69. Peng, X.L.; Yuan, W.; Zou, J.X.; Wang, B.; Hu, W.Y.; Xiong, Y. Nitrogen-incorporated ultrananocrystalline diamond/multilayer graphene composite carbon films: Synthesis and electrochemical performances. *Electrochim. Acta* **2017**, *257*, 504–509, doi:10.1016/j.electacta.2017.08.093.
70. Pop, A.; Lung, S.; Orha, C.; Manea, F. Silver/graphene-modified Boron Doped Diamond Electrode for Selective Detection of Carbaryl and Paraquat from Water. *Int. J. Electrochem. Sci.* **2018**, *13*, 2651–2660, doi:10.20964/2018.03.02.

71. Pop, A.; Manea, F.; Flueras, A.; Schoonman, J. Simultaneous Voltammetric Detection of Carbaryl and Paraquat Pesticides on Graphene-Modified Boron-Doped Diamond Electrode. *SENSORS* **2017**, *17*, doi:10.3390/s17092033.
72. Tan, S.M.; Poh, H.L.; Sofer, Z.; Pumera, M. Boron-doped graphene and boron-doped diamond electrodes: detection of biomarkers and resistance to fouling. *Analyst* **2013**, *138*, 4885–4891, doi:10.1039/c3an00535f.
73. Yuan, Q.L.; Liu, Y.; Ye, C.; Sun, H.Y.; Dai, D.; Wei, Q.P.; Lai, G.S.; Wu, T.Z.; Yu, A.M.; Fu, L.; et al. Highly stable and regenerative graphene-diamond hybrid electrochemical biosensor for fouling target dopamine detection. *Biosens. Bioelectron.* **2018**, *111*, 117–123, doi:10.1016/j.bios.2018.04.006.
74. Dettlaff, A.; Jakobczyk, P.; Sobaszek, M.; Ficek, M.; Dec, B.; Luczkiewicz, A.; Szala, M.; Wojtas, J.; Ossowski, T.; Bogdanowicz, R. Electrochemical Detection of 4,4 ′,5,5 ′-Tetranitro-1H,1 ′ H-2,2 ′-Biimidazole on Boron-Doped Diamond/Graphene Nanowall Electrodes. *IEEE Sens. J.* **2020**, *20*, 9637–9643, doi:10.1109/JSEN.2020.2973451.
75. Jiang, M.Y.; Ma, W.C.; Han, S.J.; Chen, C.K.; Fan, D.; Li, X.; Hu, X.J. Microstructure and electrochemical properties of nanocrystalline diamond and graphene hybridized films. *J. Appl. Phys.* **2020**, *127*, doi:10.1063/1.5119989.
76. Qi, X.J.; Wang, T.; Long, Y.J.; Ni, J.R. Synergetic antibacterial activity of reduced graphene oxide and boron doped diamond anode in three dimensional electrochemical oxidation system. *Sci. Rep.* **2015**, *5*, doi:10.1038/srep10388.
77. Bouchet, M.I.D.; Martin, J.M.; Avila, J.; Kano, M.; Yoshida, K.; Tsuruda, T.; Bai, S.; Higuchi, Y.; Ozawa, N.; Kubo, M.; et al. Diamond-like carbon coating under oleic acid lubrication: Evidence for graphene oxide formation in superlow friction. *Sci. Rep.* **2017**, *7*, doi:10.1038/srep46394.
78. Sealy, C. Diamond puts a new shine on friction-free graphene. *Nano Today* **2015**, *10*, 412–413, doi:10.1016/j.nantod.2015.06.003.
79. Yi, S.; Chen, X.C.; Li, J.J.; Liu, Y.F.; Ding, S.L.; Luo, J.B. Macroscale superlubricity of Si-doped diamond-like carbon film enabled by graphene oxide as additives. *Carbon N. Y.* **2021**, *176*, 358–366, doi:10.1016/j.carbon.2021.01.147.
80. Liu, Y.H.; Chen, L.; Jiang, B.Z.; Liu, Y.Q.; Zhang, B.; Xiao, C.; Zhang, J.Y.; Qian, L.M. Origin of low friction in hydrogenated diamond-like carbon films due to graphene nanoscroll formation depending on sliding mode: Unidirection and reciprocation. *Carbon N. Y.* **2021**, *173*, 696–704, doi:10.1016/j.carbon.2020.11.039.
81. Chen, S.L.; Shen, B.; Chen, Y.S.; Sun, F.H. Synergistic friction-reducing and anti-wear behaviors of graphene with micro- and nano-crystalline diamond films. *Diam. Relat. Mater.* **2017**, *73*, 25–32, doi:10.1016/j.diamond.2016.11.012.
82. Chen, S.L.; Shen, B.; Sun, F.H. The influence of normal load on the tribological performance of electrophoretic deposition prepared graphene coating on micro-crystalline diamond surface. *Diam. Relat. Mater.* **2017**, *76*, 50–57, doi:10.1016/j.diamond.2017.04.008.
83. Shen, B.; Chen, S.L.; Chen, Y.S.; Sun, F.H. Enhancement on the tribological performance of diamond films by utilizing graphene coating as a solid lubricant. *Surf. Coat. Technol.* **2017**, *311*, 35–45, doi:10.1016/j.surfcoat.2016.12.094.
84. Shen, B.; Chen, S.L.; Huang, Z.W.; Ji, Z.; Lin, Q.; Zhang, Z.N. Elucidating the atomic mechanism of the lubricity of graphene on the diamond substrate. *Appl. Surf. Sci.* **2020**, *504*, doi:10.1016/j.apsusc.2019.144372.
85. Wang, J.J.; Li, L.; Yang, W.T.; Li, M.; Guo, P.; Zhao, B.; Yang, L.F.; Fang, L.L.; Sun, B.; Jia, Y. The Flexible Lubrication Performance of Graphene Used in Diamond Interface as a Solid Lubricant: First-Principles Calculations. *NANOMATERIALS* **2019**, *9*, doi:10.3390/nano9121784.
86. Li, J.H.; Peng, Y.; Tang, X.Q.; Xu, Q.; Liu, B.; Bai, L.C. Lubrication Performance of Hydrogenated Graphene on Diamond-Like Carbon Films Based on Molecular Dynamics Simulation. *Tribol. Lett.* **2021**, *69*, doi:10.1007/s11249-020-01382-x.
87. Zhao, S.N.; Larsson, K. First principle study of the attachment of graphene onto non-doped and doped diamond (111). *Diam. Relat. Mater.* **2016**, *66*, 52–60, doi:10.1016/j.diamond.2016.03.017.
88. Zhao, S.; Larsson, K. First Principle Study of the Attachment of Graphene onto Different Terminated Diamond (111) Surfaces. *Adv. Condens. MATTER Phys.* **2019**, *2019*, doi:10.1155/2019/9098256.
89. Zhang, L.L.; Pu, J.B.; Wang, L.P.; Xue, Q.J. Frictional dependence of graphene and carbon nanotube in diamond-like carbon/ionic liquids hybrid films in vacuum. *Carbon N. Y.* **2014**, *80*, 734–745, doi:10.1016/j.carbon.2014.09.022.
90. Zhang, J.; Osloub, E.; Siddiqui, F.; Zhang, W.X.; Ragab, T.; Basaran, C. Anisotropy of Graphene Nanoflake Diamond Interface Frictional Properties. *Materials (Basel).* **2019**, *12*, doi:10.3390/ma12091425.
91. Machado, A.S.; Maroudas, D.; Muniz, A.R. Tunable mechanical properties of diamond superlattices generated by interlayer bonding in twisted bilayer graphene. *Appl. Phys. Lett.* **2013**, *103*, doi:10.1063/1.4813271.
92. Rysaeva, L.K.; Lisovenko, D.S.; Gorodtsov, V.A.; Baimova, J.A. Stability, elastic properties and deformation behavior of graphene-based diamond-like phases. *Comput. Mater. Sci.* **2020**, *172*, doi:10.1016/j.commatsci.2019.109355.
93. Yin, N.; Zhang, Z.N.; Zhang, J.Y. Frictional Contact Between the Diamond Tip and Graphene Step Edges. *Tribol. Lett.* **2019**, *67*, doi:10.1007/s11249-019-1190-7.
94. Zhao, F.; Nguyen, T.T.; Golsharifi, M.; Amakubo, S.; Loh, K.P.; Jackman, R.B. Electronic properties of graphene-single crystal diamond heterostructures. *J. Appl. Phys.* **2013**, *114*, doi:10.1063/1.4816092.
95. Zhao, F.; Nguyen, T.T.; Golsharifi, M.; Amakubo, S.; Loh, K.P.; Jackman, R.B. Electronic properties of graphene-single crystal diamond heterostructures (vol 114, 053709, 2013). *J. Appl. Phys.* **2014**, *116*, doi:10.1063/1.4894711.
96. Wang, Y.; Jaiswal, M.; Lin, M.; Saha, S.; Ozyilmaz, B.; Loh, K.P. Electronic Properties of Nanodiamond Decorated Graphene. *ACS Nano* **2012**, *6*, 1018–1025, doi:10.1021/nn204362p.

97. Hu, X.J.; Chen, C.K.; Lu, S.H. High mobility n-type conductive ultrananocrystalline diamond and graphene nanoribbon hybridized carbon films. *Carbon N. Y.* **2016**, *98*, 671–680, doi:10.1016/j.carbon.2015.11.057.
98. Bogdanowicz, R.; Ficek, M.; Sobaszek, M.; Nosek, A.; Golunski, L.; Karczewski, J.; Jaramillo-Botero, A.; Goddard, W.A.; Bockrath, M.; Ossowski, T. Growth and Isolation of Large Area Boron-Doped Nanocrystalline Diamond Sheets: A Route toward Diamond-on-Graphene Heterojunction. *Adv. Funct. Mater.* **2019**, *29*, doi:10.1002/adfm.201805242.
99. Hu, W.; Li, Z.Y.; Yang, J.L. Diamond as an inert substrate of graphene. *J. Chem. Phys.* **2013**, *138*, doi:10.1063/1.4789420.
100. Hu, Y.X.; Li, D.F.; Yin, Y.; Li, S.C.; Ding, G.Q.; Zhou, H.B.; Zhang, G. The important role of strain on phonon hydrodynamics in diamond-like bi-layer graphene. *Nanotechnology* **2020**, *31*, doi:10.1088/1361-6528/ab8ee1.
101. Khan, A.H.; Schirmann, E.; Kovi, K.K. Fluorinated graphene oxide, nanocrystalline diamond multilayer thin films for optical and electromagnetic limiting applications. *EMERGENT Mater.* **2021**, *4*, 525–530, doi:10.1007/s42247-021-00217-2.
102. Konabe, S.; Cuong, N.T.; Otani, M.; Okada, S. High-Efficiency Photoelectric Conversion in Graphene-Diamond Hybrid Structures: Model and First-Principles Calculations. *Appl. Phys. EXPRESS* **2013**, *6*, doi:10.7567/APEX.6.045104.
103. Luo, B.R.; Yuan, A.H.; Yang, S.; Han, L.Q.; Guan, R.; Duan, J.X.; Wang, C.; Dong, L.; Zhang, B.; Li, D.J. Synthesis of Diamond-like Carbon as a Dielectric Platform for Graphene Field Effect Transistors. *ACS Appl. NANO Mater.* **2021**, *4*, 1385–1393, doi:10.1021/acsanm.0c02930.
104. Wu, Y.Q.; Lin, Y.M.; Bol, A.A.; Jenkins, K.A.; Xia, F.N.; Farmer, D.B.; Zhu, Y.; Avouris, P. High-frequency, scaled graphene transistors on diamond-like carbon. *Nature* **2011**, *472*, 74–78, doi:10.1038/nature09979.
105. Ma, Y.D.; Dai, Y.; Guo, M.; Huang, B.B. Graphene-diamond interface: Gap opening and electronic spin injection. *Phys. Rev. B* **2012**, *85*, doi:10.1103/PhysRevB.85.235448.
106. Tzeng, Y.H.; Chen, Y.R.; Li, P.Y.; Chang, C.C.; Chu, Y.C. NV Center Charge State Controlled Graphene-on-Diamond Field Effect Transistor Actions With Multi-Wavelength Optical Inputs. *IEEE OPEN J. Nanotechnol.* **2020**, *1*, 18–24, doi:10.1109/OJNANO.2020.2993007.
107. Yu, J.; Liu, G.X.; Sumant, A. V; Goyal, V.; Balandin, A.A. Graphene-on-Diamond Devices with Increased Current-Carrying Capacity: Carbon sp(2)-on-sp(3) Technology. *NANO Lett.* **2012**, *12*, 1603–1608, doi:10.1021/nl204545q.
108. Loh, G.C.; Teo, E.H.T.; Tay, B.K. Compounded effect of vacancy on interfacial thermal transport in diamond-graphene nanostructures. *Diam. Relat. Mater.* **2011**, *20*, 1137–1142, doi:10.1016/j.diamond.2011.06.019.
109. Mirabedini, P.S.; Debnath, B.; Neupane, M.R.; Greaney, P.A.; Birdwell, A.G.; Ruzmetov, D.; Crawford, K.G.; Shah, P.; Weil, J.; Ivanov, T.G. Structural and electronic properties of 2D (graphene, hBN)/H-terminated diamond (100) heterostructures. *Appl. Phys. Lett.* **2020**, *117*, doi:10.1063/5.0020620.
110. Muniz, A.R.; Maroudas, D. Opening and tuning of band gap by the formation of diamond superlattices in twisted bilayer graphene. *Phys. Rev. B* **2012**, *86*, doi:10.1103/PhysRevB.86.075404.
111. Selli, D.; Baburin, I.; Leoni, S.; Zhu, Z.; Tomanek, D.; Seifert, G. Theoretical investigation of the electronic structure and quantum transport in the graphene-C(111) diamond surface system. *J. PHYSICS-CONDENSED MATTER* **2013**, *25*, doi:10.1088/0953-8984/25/43/435302.
112. Shiga, T.; Konabe, S.; Shiomi, J.; Yamamoto, T.; Maruyama, S.; Okada, S. Graphene-diamond hybrid structure as spin-polarized conducting wire with thermally efficient heat sinks. *Appl. Phys. Lett.* **2012**, *100*, doi:10.1063/1.4725485.
113. Ueda, K.; Aichi, S.; Asano, H. Photo-controllable memristive behavior of graphene/diamond heterojunctions. *Appl. Phys. Lett.* **2016**, *108*, doi:10.1063/1.4953200.
114. Ueda, K.; Mizuno, Y.; Asano, H. Multibit optoelectronic memory using graphene/diamond (carbon sp(2)-sp(3)) heterojunctions and its arithmetic functions. *Appl. Phys. Lett.* **2020**, *117*, doi:10.1063/5.0013795.
115. Wan, G.; Panditharatne, S.; Fox, N.A.; Cattelan, M. Graphene-diamond junction photoemission microscopy and electronic interactions. *NANO EXPRESS* **2020**, *1*, doi:10.1088/2632-959X/aba443.
116. Banerjee, D.; Sankaran, K.J.; Deshmukh, S.; Ficek, M.; Bhattacharya, G.; Ryl, J.; Phase, D.M.; Gupta, M.; Bogdanowicz, R.; Lin, I.N.; et al. 3D Hierarchical Boron-Doped Diamond-Multilayered Graphene Nanowalls as an Efficient Supercapacitor Electrode. *J. Phys. Chem. C* **2019**, *123*, 15458–15466, doi:10.1021/acs.jpcc.9b03628.
117. Cui, D.D.; Li, H.J.; Li, M.J.; Li, C.P.; Qian, L.R.; Zhou, B.Z.; Yang, B.H. Boron-Doped Graphene Directly Grown on Boron-Doped Diamond for High-Voltage Aqueous Supercapacitors. *ACS Appl. ENERGY Mater.* **2019**, *2*, 1526-+, doi:10.1021/acsaem.8b02120.
118. Sun, Y.Q.; Wu, Q.O.; Xu, Y.X.; Bai, H.; Li, C.; Shi, G.Q. Highly conductive and flexible mesoporous graphitic films prepared by graphitizing the composites of graphene oxide and nanodiamond. *J. Mater. Chem.* **2011**, *21*, 7154–7160, doi:10.1039/c0jm04434b.
119. Wang, Q.; Plylahan, N.; Shelke, M. V; Devarapalli, R.R.; Li, M.S.; Subramanian, P.; Djenizian, T.; Boukherroub, R.; Szunerits, S. Nanodiamond particles/reduced graphene oxide composites as efficient supercapacitor electrodes. *Carbon N. Y.* **2014**, *68*, 175–184, doi:10.1016/j.carbon.2013.10.077.
120. Tzeng, Y.H.; Chen, W.L.; Wu, C.H.; Lo, J.Y.; Li, C.Y. The synthesis of graphene nanowalls on a diamond film on a silicon substrate by direct-current plasma chemical vapor deposition. *Carbon N. Y.* **2013**, *53*, 120–129, doi:10.1016/j.carbon.2012.10.038.
121. Benfante, A.; Tomada, A.; Carini, G.A.; IEEE Novel diamond X-ray detectors with patterned reduced graphene oxide contacts.

In *2015 IEEE NUCLEAR SCIENCE SYMPOSIUM AND MEDICAL IMAGING CONFERENCE (NSS/MIC)*; 2015 ISBN 1095-7863.

122. Brenneis, A.; Gaudreau, L.; Seifert, M.; Karl, H.; Brandt, M.S.; Huebl, H.; Garrido, J.A.; Koppens, F.H.L.; Holleitner, A.W. Ultrafast electronic readout of diamond nitrogen-vacancy centres coupled to graphene. *Nat. Nanotechnol.* **2015**, *10*, 135–139, doi:10.1038/NNANO.2014.276.
123. Qiao, Y.; Qi, T.; Liu, J.; He, Z.Y.; Yu, S.W.; Shen, Y.Y.; Hei, H.J. SYNTHESIS OF GRAPHENE/DIAMOND DOUBLE-LAYERED STRUCTURE FOR IMPROVING ELECTRON FIELD EMISSION PROPERTIES. *Surf. Rev. Lett.* **2016**, *23*, doi:10.1142/S0218625X16500116.
124. Sankaran, K.J.; Chang, T.H.; Bikkarolla, S.K.; Roy, S.S.; Papakonstantinou, P.; Drijkoningen, S.; Pobedinskas, P.; Van Bael, M.K.; Tai, N.H.; Lin, I.N.; et al. Growth, structural and plasma illumination properties of nanocrystalline diamond-decorated graphene nanoflakes. *RSC Adv.* **2016**, *6*, 63178–63184, doi:10.1039/c6ra07116c.
125. Sankaran, K.J.; Ficek, M.; Kunuku, S.; Panda, K.; Yeh, C.J.; Park, J.Y.; Sawczak, M.; Michalowski, P.P.; Leou, K.C.; Bogdanowicz, R.; et al. Self-organized multi-layered graphene-boron-doped diamond hybrid nanowalls for high-performance electron emission devices. *Nanoscale* **2018**, *10*, 1345–1355, doi:10.1039/c7nr06774g.
126. Sankaran, K.J.; Yeh, C.J.; Drijkoningen, S.; Pobedinskas, P.; Van Bael, M.K.; Leou, K.C.; Lin, I.N.; Haenen, K. Enhancement of plasma illumination characteristics of few-layer graphene-diamond nanorods hybrid. *Nanotechnology* **2017**, *28*, doi:10.1088/1361-6528/aa5378.
127. Varshney, D.; Rao, C. V; Guinel, M.J.F.; Ishikawa, Y.; Weiner, B.R.; Morell, G. Free standing graphene-diamond hybrid films and their electron emission properties. *J. Appl. Phys.* **2011**, *110*, doi:10.1063/1.3627370.
128. Yamada, T.; Masuzawa, T.; Mimura, H.; Okano, K. Field emission spectroscopy measurements of graphene/n-type diamond heterojunction. *Appl. Phys. Lett.* **2019**, *114*, doi:10.1063/1.5094365.
129. Yamada, T.; Masuzawa, T.; Neo, Y.; Mimura, H.; Ogawa, S.; Takakuwa, Y.; Okano, K. Field emission from n-type diamond NEA surface and graphene/n-type diamond junction. In *2017 30TH INTERNATIONAL VACUUM NANOELECTRONICS CONFERENCE (IVNC)*; Langer, C., Lawrowski, R., Eds.; 2017; pp. 20–21 ISBN 2164-2370.
130. Santos, N.F.; Zubets, U.; Carvalho, A.F.; Fernandes, A.J.S.; Pereira, L.; Costa, F.M. Tuning the field emission of graphene-diamond hybrids by pulsed methane flow CVD. *Carbon N. Y.* **2017**, *122*, 726–736, doi:10.1016/j.carbon.2017.07.024.
131. Yang, J.; Tang, L.L.; Luo, W.; Feng, S.L.; Leng, C.Q.; Shi, H.F.; Wei, X.Z. Interface Engineering of a Silicon/Graphene Heterojunction Photodetector via a Diamond-Like Carbon Interlayer. *ACS Appl. Mater. Interfaces* **2021**, *13*, 4692–4702, doi:10.1021/acsami.0c18850.
132. Huang, B.R.; Saravanan, A.; Lu, H.C. Structural Engineering of Dispersed Graphene Flakes into ZnO Nanotubes on Discontinues Ultra-Nanocrystalline Diamond Substrates for High-Performance Photodetector with Excellent UV Light to Dark Current Ratios. *Adv. Mater. INTERFACES* **2020**, *7*, doi:10.1002/admi.201901694.
133. Wei, M.S.; Yao, K.Y.; Liu, Y.M.; Yang, C.; Zang, X.N.; Lin, L.W. A Solar-Blind UV Detector Based on Graphene-Microcrystalline Diamond Heterojunctions. *SMALL* **2017**, *13*, doi:10.1002/smll.201701328.
134. Yao, K.Y.; Yang, C.; Zang, X.N.; Feng, F.; Lin, L.W.; IEEE *CARBON SP2-SP3 TECHNOLOGY: GRAPHENE-ON-DIAMOND THIN FILM UV DETECTOR*; 2014; ISBN 978-1-4799-3508-6.
135. Wieghold, S.; Li, J.; Simon, P.; Krause, M.; Avlasevich, Y.; Li, C.; Garrido, J.A.; Heiz, U.; Samori, P.; Mullen, K.; et al. Photoresponse of supramolecular self-assembled networks on graphene-diamond interfaces. *Nat. Commun.* **2016**, *7*, doi:10.1038/ncomms10700.
136. Zhang, Z.L.; Huang, J.; Xi, Y.F.; Zhou, X.Y.; Tang, K.; Xia, Y.B.; Lu, Y.C.; Wang, L.J. CVD diamond film detectors for a particles with a new electrode structure of reduced graphene oxide/Au. *Mater. Sci. Semicond. Process.* **2019**, *91*, 260–266, doi:10.1016/j.mssp.2018.11.027.
137. Chen, Z.R.; Ma, D.J.; Wang, S.M.; Dai, W.H.; Li, S.Q.; Zhu, Y.Q.; Liu, B.C. Effects of graphene addition on mechanical properties of polycrystalline diamond compact. *Ceram. Int.* **2020**, *46*, 11255–11260, doi:10.1016/j.ceramint.2020.01.150.
138. Chu, B.; Shi, Y.F.; Samuel, J. Mitigation of chemical wear by graphene platelets during diamond cutting of steel. *Carbon N. Y.* **2016**, *108*, 61–71, doi:10.1016/j.carbon.2016.06.036.
139. Wang, R.; Zhang, J.H.; Chen, S.Y.; Wu, L.X.; Zhuo, D.X.; Cheng, X.Y. Green fabrication of graphene oxide/epoxy nanocomposite and its application in diamond abrasive tools. *Compos. PART B-ENGINEERING* **2019**, *177*, doi:10.1016/j.compositesb.2019.107383.
140. Duan, D.Z.; Ma, Y.S.; Ding, J.J.; Chang, Z.D.; Liu, H.B.; Xu, L.; Jiang, Z.D. Effect of multilayer graphene addition on performance of brazed diamond drill bits with Ni-Cr alloy and its mechanism. *Ceram. Int.* **2020**, *46*, 16684–16692, doi:10.1016/j.ceramint.2020.03.242.
141. Duan, D.Z.; Li, C.S.; Sun, L.; Liu, Y.P.; Fang, X.D.; Lin, Q.J.; Jiang, Z.D. Microstructure and performance of brazed diamonds with Ni-Cr plus multilayer graphene composite alloy. *J. Alloys Compd.* **2020**, *816*, doi:10.1016/j.jallcom.2019.152630.
142. Smith, P.J.; Chu, B.; Singh, E.; Chow, P.; Samuel, J.; Koratkar, N. Graphene oxide colloidal suspensions mitigate carbon diffusion during diamond turning of steel. *J. Manuf. Process.* **2015**, *17*, 41–47, doi:10.1016/j.jmapro.2014.10.007.
143. Ilyas, S.U.; Ridha, S.; Sardar, S.; Estelle, P.; Kumar, A.; Pendyala, R. Rheological behavior of stabilized diamond-graphene

nanoplatelets hybrid nanosuspensions in mineral oil. *J. Mol. Liq.* **2021**, *328*, doi:10.1016/j.molliq.2021.115509.

144. Jiang, J.; Liu, F.X.; Zhuang, K.Y.; Chen, D.Q.; Chen, G.H. Composites of epoxy/graphene-modified-diamond filler show enhanced thermal conductivity and high electrical insulation. *RSC Adv.* **2017**, *7*, 40761–40766, doi:10.1039/c7ra07272d.
145. Saw, W.P.S.; Mariatti, M. Properties of synthetic diamond and graphene nanoplatelet-filled epoxy thin film composites for electronic applications. *J. Mater. Sci. Electron.* **2012**, *23*, 817–824, doi:10.1007/s10854-011-0499-2.
146. Bittencourt, R.A.; Costa, G.D.; Lima, A.T.D.; Lima, I.C.D. Cluster formation and non-metal-to-metal transition in a diamond-shaped graphene-like lattice. *AIP Adv.* **2021**, *11*, doi:10.1063/5.0040573.
147. Yu, J.H.; Qian, R.; Jiang, P.K. Enhanced Thermal Conductivity for PVDF Composites with a Hybrid Functionalized Graphene Sheet-Nanodiamond Filler. *FIBERS Polym.* **2013**, *14*, 1317–1323, doi:10.1007/s12221-013-1317-7.
148. Shul'zhenko, A.A.; Jaworska, L.; Gargin, V.G.; Sokolov, A.N.; Nikolenko, A.S.; Strelchuk, V. V Dry mixing of diamond and n-layered graphene powders substantially different in density and particle size. *HIGH Press. Res.* **2018**, *38*, 53–61, doi:10.1080/08957959.2017.1396325.
149. Zhou, F.; Chen, N.C.; Ju, F.S. Enhanced Growth Rate of Chemical Vapor Deposition Diamond Coating Motivated by Graphene Oxide. *COATINGS* **2021**, *11*, doi:10.3390/coatings11050559.
150. Tzeng, Y.H.; Yeh, S.P.; Fang, W.C.; Chu, Y.C. Nitrogen-incorporated ultrananocrystalline diamond and multi-layer-graphene-like hybrid carbon films. *Sci. Rep.* **2014**, *4*, doi:10.1038/srep04531.
151. Lowe, S.E.; Shi, G.; Zhang, Y.B.; Qin, J.D.; Wang, S.J.; Uijtendaal, A.; Sun, J.Q.; Jiang, L.X.; Jiang, S.Y.; Qi, D.C.; et al. Scalable Production of Graphene Oxide Using a 3D-Printed Packed-Bed Electrochemical Reactor with a Boron-Doped Diamond Electrode. *ACS Appl. NANO Mater.* **2019**, *2*, 867–878, doi:10.1021/acsanm.8b02126.
152. Lan, G.J.; Qiu, Y.Y.; Fan, J.T.; Wang, X.L.; Tang, H.D.; Han, W.F.; Liu, H.Z.; Liu, H.Y.; Song, S.; Li, Y. Defective graphene@diamond hybrid nanocarbon material as an effective and stable metal-free catalyst for acetylene hydrochlorination. *Chem. Commun.* **2019**, *55*, 1430–1433, doi:10.1039/c8cc09361j.
153. Roldan, L.; Benito, A.M.; Garcia-Bordeje, E. Self-assembled graphene aerogel and nanodiamond hybrids as high performance catalysts in oxidative propane dehydrogenation. *J. Mater. Chem. A* **2015**, *3*, 24379–24388, doi:10.1039/c5ta07404e.
154. Zang, J.B.; Wang, Y.H.; Bian, L.Y.; Zhang, J.H.; Meng, F.W.; Zhao, Y.L.; Lu, R.; Qu, X.H.; Ren, S.B. Graphene growth on nanodiamond as a support for a Pt electrocatalyst in methanol electro-oxidation. *Carbon N. Y.* **2012**, *50*, 3032–3038, doi:10.1016/j.carbon.2012.02.089.
155. Kayal, A.; Chandra, A. Infrared Spectral and Dynamical Properties of Water Confined in Nanobubbles at Hybrid Interfaces of Diamond and Graphene: A Molecular Dynamics Study. *J. Phys. Chem. C* **2017**, *121*, 23455–23462, doi:10.1021/acs.jpcc.7b06911.
156. Lim, C.; Sorkin, A.; Bao, Q.L.; Li, A.; Zhang, K.; Nesladek, M.; Loh, K.P. A hydrothermal anvil made of graphene nanobubbles on diamond. *Nat. Commun.* **2013**, *4*, doi:10.1038/ncomms2579.